

**SPATIO-TEMPORAL ANALYSIS OF METEOROLOGICAL VARIABLES OVER
INDIA FOR 21st CENTURY: APPROACH WITH CMIP6 CLIMATE MODELS**

By

ASHITHA MARIYA SHAJI (2020-02-028)

HARIPRIYA H (2020-02-029)

ANUSHA C RAJESH (2020-02-030)

ADHITHYA P B (2020-02-043)



**DEPARTMENT OF IRRIGATION AND DRAINAGE ENGINEERING
KELAPPAJI COLLEGE OF AGRICULTURAL ENGINEERING AND
TECHNOLOGY**

TAVANUR-679573, MALAPPURAM

KERALA, INDIA

2024

**SPATIO-TEMPORAL ANALYSIS OF METEOROLOGICAL VARIABLES OVER
INDIA FOR 21st CENTURY: APPROACH WITH CMIP6 CLIMATE MODELS**

By

ASHITHA MARIYA SHAJI (2020-02-028)

HARIPRIYA H (2020-02-029)

ANUSHA C RAJESH (2020-02-030)

ADHITHYA P B (2020-02-043)

PROJECT REPORT

Submitted in partial fulfilment of the requirement for the degree of

Bachelor of Technology

In

Agricultural Engineering

Faculty of Agricultural Engineering and Technology

Kerala Agricultural University



DEPARTMENT OF IRRIGATION AND DRAINAGE ENGINEERING

KELAPPAJI COLLEGE OF AGRICULTURAL ENGINEERING AND

TECHNOLOGY

TAVANUR-679573, MALAPPURAM

KERALA, INDIA

2024

DECLARATION

We hereby declare that this project entitled “**SPATIO-TEMPORAL ANALYSIS OF METEOROLOGICAL VARIABLES OVER INDIA FOR 21st CENTURY: APPROACH WITH CMIP6 CLIMATE MODELS**” is a bonafide record of project work done by us during the course of study and that the report has not previously formed the basis for the award to us of any degree, diploma, associate ship, fellowship or other similar title of another university or society.

Place: Tavanur

Date: 31.05.2024

ASHITHA MARIYA SHAJI

(2020-02-028)

HARIPRIYA H

(2020-02-029)

ANUSHA C RAJESH

(2020-02-030)

ADHITHYA P B

(2020-02-043)

CERTIFICATE

Certified that the project entitled “**SPATIO-TEMPORAL ANALYSIS OF METEOROLOGICAL VARIABLES OVER INDIA FOR 21st CENTURY: APPROACH WITH CMIP6 CLIMATE MODELS**” is a record of project work done jointly by Ms. Ashitha Mariya Shaji (2020-02-028), Ms. Haripriya H (2020-02-029), Ms. Anusha C Rajesh (2020-02-030), Ms. Adhithya P B (2020-02-043) under my guidance and supervision and that it has not previously formed the basis for the award of any degree, diploma, fellowship or associateship to them.

Place: Tavanur

Date: 31.05.2024

Guide	: Dr. Rema K P Professor & Head Dept of IDE KCAET, Tavanur
Co- Guide	: Dr. Kanthavel P Asst. Professor (C) Dept of IDE KCAET, Tavanur

ACKNOWLEDGEMENT

Any project work requires the efforts of many people, and our work is no different. We are thankful to **Dr. Jayan P R**, Dean of faculty, KCAET, Tavanur for the support and guidance throughout the project. With due respect, we would like to express our sincere gratitude to our guide **Dr. Rema K P**, Professor & Head, Department of Irrigation and Drainage Engineering, KCAET, Tavanur for her immense encouragement, valuable advices and constant guidance throughout our endeavour. We also reflect our sense of indebtedness to co-guide Dr. Kanthavel P, Asst. Professor (C), Department of Irrigation and Drainage Engineering, KCAET, Tavanur, for imparting his skills towards the fulfilment of our project. We are also contented to all the faculties of Department of Irrigation and Drainage Engineering, KCAET, Tavanur.

We also express our gratitude to **Dr. Abdul Hakkim V.M**, HOD, Department of Soil and Water Conservation Engineering, KCAET, Tavanur. Dr.Sathian K.K Professor of Soil and Water Conservation Engineering, KCAET, Tavanur. We extend our sincere gratitude to our college and the Kerala Agricultural University for all the facilities provided to us. Despite of all, we are grateful to almighty for the blessings bestowed upon us. We also wish to remember our parents, who always bless us for our betterment and pray for our success. Finally, we thank all those, who directly or indirectly helped us, emphasizing the collaborative efforts of the team members as well.

ASHITHA MARIYA SHAJI (2020-02-028)

HARIPRIYA H (2020-02-029)

ANUSHA C RAJESH (2020-02-030)

ADHITHYA P B (2020-02-043)

*DEDICATED TO OUR
PROFESSION*

TABLE OF CONTENTS

CHAPTER NO.	TITLE	PAGE NO.
	LIST OF TABLES	i
	LIST OF FIGURES	ii
	SYMBOLS AND ABBREVIATIONS	vi
I	INTRODUCTION	1
II	REVIEW OF LITERATURE	6
III	MATERIALS & METHODS	17
IV	RESULTS & DISCUSSION	30
V	SUMMARY & CONCLUSION	65
	REFERENCES	68
	APPENDICES	
	ABSTRACT	

LIST OF TABLES

Table		
No.	Title	Page No.
3.1	List of selected cities with their corresponding Koppen climatic zone	19
3.2	Data source with spatial resolution and timespan	21
3.3	List of CMIP6 models used in this study along with the country of origin	22
4.1	Result of the model analysis for the region Amw	31
4.2	Suitable model for different climatic regions	32
4.3	Trends in precipitation and temperature for entire India under four SSP scenarios for the time period 2024-2100	33
4.4	Coefficient of variation (C.V.) of the future precipitation	53

LIST OF FIGURES

Figure No.	Title	Page No.
3.1	Koppen's climatic classification- India	20
3.2	ArcGIS	22
3.3	MATLAB	22
3.4	Flow chart for the identification of suitable climatic model	23
3.5	Flow chart for the trend analysis of meteorological variables	25
3.6	Flow chart for the identification of change point in upcoming time period	27
3.7	Flow chart for the comparison of future time series of meteorological variables using wavelet coherence	29
PRECIPITATION		
4.1	Z value for trend analysis using historical data	36
4.2	Sen's slope value for trend analysis using historical data	36
4.3	SSP 1 near future Z value	37
4.4	SSP 1 far future Z value	37
4.5	SSP 1 near future Sen's slope value	37
4.6	SSP 1 far future Sen's slope value	37
4.7	SSP 2 near future Z value	38
4.8	SSP 2 far future Z value	38
4.9	SSP 2 near future Sen's slope value	38
4.10	SSP 2 far future Sen's slope value	38
4.11	SSP 3 near future Z value	39
4.12	SSP 3 far future Z value	39
4.13	SSP 3 near future Sen's slope value	39
4.14	SSP 3 far future Sen's slope value	39
4.15	SSP 5 near future Z value	40

4.16	SSP 5 far future Z value	40
4.17	SSP 5 near future Sen's slope value	41
4.18	SSP 5 far future Sen's slope value	41
MAXIMUM TEMPERATURE		
4.19	Z value for trend analysis using historical data	42
4.20	Sen's slope value for trend analysis using historical data	42
4.21	SSP 1 near future Z value	43
4.22	SSP 1 far future Z value	43
4.23	SSP 1 near future Sen's slope value	43
4.24	SSP 1 far future Sen's slope value	43
4.25	SSP 2 near future Z value	44
4.26	SSP 2 far future Z value	44
4.27	SSP 2 near future Sen's slope value	44
4.28	SSP 2 far future Sen's slope value	44
4.29	SSP 3 near future Z value	45
4.30	SSP 3 far future Z value	45
4.31	SSP 3 near future Sen's slope value	45
4.32	SSP 3 Far future Sen's slope value	45
4.33	SSP 5 near future Z value	46
4.34	SSP 5 far future Z value	46
4.35	SSP 5 near future Sen's slope value	46
4.36	SSP 5 far future Sen's slope value	46
MINIMUM TEMPERATURE		
4.37	Z value for trend analysis using historical data	47

4.38	Sen's slope value for trend analysis using historical data	47
4.39	SSP 1 near future Z value	48
4.40	SSP 1 far future Z value	48
4.41	SSP 1 near future Sen's slope value	48
4.42	SSP 1 far future Sen's slope value	48
4.43	SSP 2 near future Z value	49
4.44	SSP 2 far future Z value	49
4.45	SSP 2 near future Sen's slope value	49
4.46	SSP 2 far future Sen's slope value	49
4.47	SSP 3 near future Z value	50
4.48	SSP 3 far future Z value	50
4.49	SSP 3 near future Sen's slope value	50
4.50	SSP 3 far future Sen's slope value	50
4.51	SSP 5 near future Z value	51
4.52	SSP 5 far future Z value	51
4.53	SSP 5 near future Sen's slope value	52
4.54	SSP 5 far future Sen's slope value	52
4.55	Change point analysis of future data for SSP1 (A) Precipitation (B) T max (C) Tmin	54
4.56	Change point analysis of future data for SSP2 (A) Precipitation (B) T max (C) Tmin	56
4.57	Change point analysis of future data for SSP3	57

	(A) Precipitation (B) T max (C) Tmin	
4.58	Change point analysis of future data for SSP5	59
	(A) Precipitation (B) T max (C) Tmin	
4.59	Wavelet coherence plot of region 1-Amw	60
4.60	Wavelet coherence plot of region 2-As	60
4.61	Wavelet coherence plot of region 4-Bshw	61
4.62	Wavelet coherence plot of region 5-Bwhw	62
4.63	Wavelet coherence plot of region 6-Cwg	62
4.64	Wavelet coherence plot of region 7-Dfc	63
4.65	Wavelet coherence plot of region 8-E	63

SYMBOLS & ABBREVIATIONS

&	:- And
°	:- Degree
'	:- Minute
"	:- Seconds
%	:- Percentage
ANOVA	:- Analysis of Variance
AO	:- Arctic Oscillation
ArcGIS	:- Aeronautical Reconnaissance Coverage Geographic Information
CMIP6	:- Coupled Model Inter Comparison Project Phase 6
et al	:- And others
GCMs	:- Global Climate Models
GHGs	:- Greenhouse Gases
GIS	:- Geographic Information System
IDW	:- Inverse Distance Weightage
IMD	:- India Meteorological Department
IOD	:- Indian Ocean Dipole
IPCC	:- Intergovernmental Panel on Climate Change
ISMI	:- Indian Summer Monsoon Index
MBE	:- Mean Bias Error
MEI	:- Multivariate ENSO Index
NAO	:- North Atlantic Oscillation
NDVI	:- Normalized Difference Vegetation Index
PDO	:- Pacific Decadal Oscillation
RCP	:- Representative Concentration Pathway
RDI	:- Reconnaissance Drought Index
RMSE	:- Root Mean Square Error

SD	:- Standard Deviation
SDI	:-Streamflow Drought Index
SIF	:- Solar-induced Chlorophyll Fluorescence
SOI	:- Southern Oscillation Index
SPI	:- Standardized Precipitation Index
SSP	:- Shared Socioeconomic Pathway
Wm⁻²	:- Watts per square meter

Introduction

CHAPTER I

INTRODUCTION

Climate encompasses all the physical attributes of our environment, including temperature, precipitation, air pressure, and humidity. When these factors undergo alterations, whether due to natural processes or human activities, it leads to the phenomenon known as climate change. In the twenty-first century, climate change stands out as a paramount global challenge. Its repercussions are expected to intensify over time. The escalating risk of food shortages due to climate change is a matter of great concern, presenting multifaceted threats to global food production. These challenges are further compounded by the scarcity of freshwater resources, a problem projected to worsen in the future. Climate change also contributes to a range of environmental hazards, including the increased frequency of extreme events such as floods and droughts. Climate change, driven by the increase in global temperatures has significant impacts on various areas like human health, rising sea levels, glacier melting, and alterations in precipitation patterns. Consequently, the world has witnessed a surge in severe droughts, floods, and other extreme weather events (Abbas *et al.*,2024).

Climate change affects all sectors of society due to changes in temperature and precipitation patterns and will continue to do so in the foreseeable future. Extreme weather events are already more frequent and intense, generating additional costs for businesses nationally and globally. Climate risk disclosure and management can be challenging due to the complexity of climate impacts and unpredictability of extreme events' occurrence and location.

Both the physical impacts of climate change and transitional risk stemming from policies to reduce emissions of GHGs, already affect all sectors of society. The value of assets at risk from climate change is expected to range from 4.2 to 43 trillion USD globally between now and 2100, dependent on which climate change scenario materializes. Shifts in temperature and precipitation patterns can affect crop yields and consequently, food security. Extreme weather events can cause substantial physical damage to buildings and critical infrastructure along with economic damage, leading to reduced economic growth.

Scenarios are coherent narratives that describe plausible future outcomes and are used to identify and assess climate implications based on a range of assumptions regarding future GHG emissions, demography, and socio-economic development. The inclusion of high-warming and low-warming climate change scenarios allows for consideration of different levels of climate change impacts. Disasters emanating from climate change are a significant worry, but the manner in which it is intertwined with political processes is deeply rooted in social and structural context—more so in the South. Climate induced disaster policies in South Asia have attracted significant interest in research and advocacy and thus occupy prominent positions at both state and district levels (Torvanger *et al.*,2024).

The extreme precipitation events are evident and prominent worldwide, including the Indian region, which causes a significant impact on agriculture, loss of land, migration of people, etc. Indian agriculture and economy are dependent on summer monsoon occurrence, which accounts for nearly more than 75% of yearly rainfall. During Past years, India has observed several extreme precipitation events due to high variability in southwest monsoon precipitation. The International disaster databases estimated 268 severe flooding events occurred in India from 1950 to 2015, resulting in casualties of 69,000 persons, making 17 million people homeless, and impacting 825 million population. It is observed that a threefold increase in extreme precipitation events happened from 1950 to 2015. It showed that extreme rainfall events increased significantly during the time, and there is a need to understand the occurrence dynamicity and associated induced risks (Goyal *et al.*,2022).

According to Patel *et al.*, (2024), greenhouse gas (GHG) emissions significantly impact climate systems, and global climate models (GCMs) can replicate these effects to expect future conditions accurately. Using these models to simulate previous climates and predict future reactions to rising GHG emissions is widespread. The ability of GCMs to foretell future climate in response to varying scenarios of atmospheric GHG concentration is a significant benefit of these models. As part of the Coupled Model Inter-comparison Project (CMIP), the public can access these GCMs.

From the oldest to the most recent version, CMIP6, CMIP models have undergone significant development throughout the years to overcome difficulties. The GCMs of the CMIP6 differ from those of earlier CMIPs in that the most recent version offers a more

realistic portrayal of the physical processes that occur on earth. Besides this, the CMIP6 model makes projections based on other scenarios that use the Shared Socioeconomic Pathways (SSPs). These revised climate projections consider recent socioeconomic developments, technological advancements, and other environmental factors (such as land use), which pave the way for the creation of new scenarios that can be used to more accurately evaluate the effects of various climate change policies. The CMIP6 lays a strong emphasis on the coordination of experiments to get a deeper comprehension of the processes that underlie the variability of climate (Patel *et al.*,2024).

According to Leimbach *et al.*, (2023), major socio-economic drivers of long-term dynamics in models assessing climate change are taken into account by scenario assumptions. Population and GDP projections associated with the Shared SSP scenarios represent such drivers. The scenario method is a common research tool to improve the understanding of complex interactions of natural systems and human activities. While scenarios, in general, provide “plausible descriptions of how the future might unfold”, the recently introduced SSP scenario framework was developed to facilitate analyses on the impacts of climate change, as well as their mitigation and adaptation.

SSP1 (“Sustainability”) characterizes a world that makes progress towards sustainability, including the rapid development of low-income countries and relatively high urbanization rates. SSP2 as the “middle of the road Scenario” is meant to continue historical trends with a medium level of per capita GDP growth and urbanization. The narrative of SSP3 (“Regional Rivalry”) sketches a strongly fragmented world characterized by a high level of poverty, a high level of the rural population, and subject to high mitigation and adaptation challenges. SSP4 (“Inequality”) represents a highly unequal world with a strong divide of rich and poor people between countries as well as within countries. This divide additionally appears in urban areas that grow comparatively fast. Finally, SSP5 (“Fossil-fueled development”) characterizes a growth-oriented world with large technological progress and high urbanization rates. The energy supply relies largely on fossil fuel-based energy conversion technologies and therefore causes high mitigation challenges (Leimbach *et al.*,2023).

The novelty of this research lies in its comprehensive evaluation of the spatio-temporal variation of the selected meteorological variables of CMIP6 GCMs over the Indian region, which includes several unique aspects: a multi-faceted evaluation, regional

focus with unique climatic characteristics and practical implications of its findings that offer guidance for improving GCM performance in different climatic zones.

To analyse the trend, the non-parametric test (Modified Mann-Kendall test) and Sen's slope estimator were used. The modified Mann-Kendall test is a hypothesis test that determines whether a given sequence of data has a trend. It builds upon the original Mann-Kendall test but is more powerful as it can account for autocorrelations within the data. Sen's slope test is a method used to discover the nature of trends in univariate time series. It is a non-parametric method used for trend analysis and to identify trend magnitude. Pettitt's (1979) method is a rank-based nonparametric test for abrupt changes in a time series. The Pettitt test produces a supposed change-point, even when the trend is smooth, or when the abrupt change is smaller than the long-term smooth change. Wavelet coherence is a measure of the correlation between two signals. Wavelet coherence analysis is a method used to measure the cross-correlation between two signals as a function of both frequency and time. It provides insights into how two signals are related in the time-frequency plane.

The present study intends to assess the effects of climate change on the development of a sustainable climatic environment and then developed ensemble climate projections under the shared SSPs using CMIP6 data. The main objectives of our study are enlisted below:

1. Identification of suitable climatic model
2. Analysis of trend of meteorological variables with MMK and Sen's Slope test
3. Identification of change point in upcoming time period for the meteorological variables
4. Comparison of future time series of meteorological variable using Wavelet coherence

This research can suggest strategies to increase the accuracy and reliability of future climate predictions. This study concentrates on CMIP6 precipitation and extreme temperature evaluation over India, the world's most influential nation in terms of climate

Review of literature

CHAPTER II

REVIEW OF LITERATURE

This chapter contains the review of the various research conducted in the relevant aspects with respect to the objectives of the study. The reviews are grouped under the following subheads.

1. Collection and evaluation of climatic model data.
2. Trend analysis of meteorological variables using Modified Mann-Kendall and Sen's Slope test.
3. Detection of change point for the meteorological variable time series by Pettit test.
4. Time series analysis of meteorological variables using Wavelet coherence.

2.1 COLLECTION AND EVALUATION OF CLIMATIC MODEL DATA

Guhathakurta and Rajeevan (2008) conducted a comprehensive analysis of rainfall patterns across 36 meteorological subdivisions of India by reconstructing monthly, seasonal, and annual rainfall time series from 1901 to 2003. Utilizing a uniform network of 1,476 rain gauge stations, they ensured extensive spatial coverage and homogeneity in the data collected. Their linear trend analysis uncovered significant variances in long-term rainfall trends: notable decreases during the south-west monsoon in Jharkhand, Chhattisgarh, and Kerala, and increases in regions like Gangetic West Bengal and Konkan and Goa, among others. The study also highlighted shifts in the contribution of individual monsoon months to annual rainfall, particularly noting a decline in June, July, and September, and an increase in August. Through EOF(Empirical Orthogonal Function) analysis, they elucidated the spatial distribution of rainfall, thus providing a robust framework for future climatological studies and water resource management in India.

Mazzoglio *et al.*,(2022) had done a comprehensive analysis of the spatial and temporal trend of short-duration (1 to 24 h) annual maximum rainfall depths, derived from the Improved Italian—Rainfall Extreme Dataset(I2-RED). The investigation is conducted using time series of at least 30 years of data both at the national and regional level using the record-breaking analysis, the Mann-Kendall test, the Regional Kendall test and the Sen's slope estimator. The results confirm that rainfall extremes of different

durations are not increasing uniformly over Italy and that separate tendencies emerge in different sectors, even at close distances.

Alemu *et al.*,(2024) undertook a comprehensive examination of the temporal and spatial patterns of meteorological and hydrological droughts within North Wollo, South Wollo, and the Oromia special zones of Ethiopia. Utilizing a variety of drought indices, including the Standardized Precipitation Index (SPI), Reconnaissance Drought Index (RDI), and Streamflow Drought Index (SDI) processed through DrinC software, the team analysed data collected from the Ethiopian Meteorology Institute and the Ministry of Water and Energy. Their historical analysis relied on thirty-two years of data from ten meteorological stations, while future projections employed (Representative Concentration Pathway) RCP 4.5 to downscale climate data and artificial neural networks for forecasting streamflow. Findings indicated that these zones experienced severe to extreme droughts with a high frequency, with notable episodes occurring almost biennially between 1984 and 1992, and predictions suggest an increase to five-year intervals in future drought occurrences. The severity and short intervals between these events highlight the urgent need for effective drought mitigation strategies and the implementation of an early warning system to safeguard the affected communities.

In another study by Dahiya *et al.*,(2024) they described that Indian Summer Monsoon Rainfall (ISMR) plays a critical role in agriculture, thereby significantly affecting the economy of India. Yet, there is a large spread in the ISMR variability for future projections (by the end of 21st century) as simulated by coupled general circulation models. Gaining insight into the variations of the ISMR during warm periods could enhance our ability to understand ISMR variability in the future. To evaluate the ISMR mean state during the mid-Pliocene, they had used six available Coupled Model Intercomparison Project phase- 6 (CMIP-6) model simulations and their multi-model ensemble mean. Their analysis suggests that the ensemble of CMIP-6 models is better than individual models in capturing the ISM rainfall patterns and its characteristics for the historical period of 1914–2013. During the mid-Pliocene, they found an increase in the June to September rainfall over most parts of India in comparison to the pre-industrial period with an increase of 34% in seasonal precipitation.

Petrova *et al.*,(2024) in their study, delves into the complexities of climate change impacts on California's winter precipitation, utilizing projections from the most recent

Coupled Model Intercomparison Project Phase-6 (CMIP-6). This research crucially highlights California as a region of major climatic uncertainty, with historical model predictions oscillating between anticipations of both wetter and drier future scenarios. Petrova and colleagues analyse mid-century and end-century precipitation projections, revealing a substantial agreement among models that northern California will experience wetter conditions. In stark contrast, southern California remains a contentious area, with an almost equal split in model predictions between wetter and drier outcomes. Notably, the projected end-century precipitation changes range significantly, from a decrease of 20% to an increase of 80% in CMIP-6, marking a shift towards generally wetter conditions and greater variability compared to CMIP-5.

2.2 TREND ANALYSIS OF METEOROLOGICAL VARIABLES USING MODIFIED MANN-KENDALL AND SEN'S SLOPE TEST

Hu and Wang (2009) rigorously examined the hydrological dynamics of Taihu Lake, emphasizing the crucial role of its annual highest water level (Z_m) in flood management within the Taihu Basin. The research extends from 1956 to 2000, applying Mann-Kendall and Spearman non-parametric tests to detect trends in areal precipitation and pan evaporation, alongside Morlet wavelet transformation to analyze fluctuation patterns. Their study also considered human influences such as land use changes and developments. A multifaceted approach using multi-linear regression models elucidates the relationship between Z_m , precipitation, and evaporation in the critical 30-day period preceding the peak water level. Results indicated that a significant rise in Z_m after 1980, attributed 83.6% to the increase of climatic factors while human activities account for 16.4%. This delineation underscores the dominant influence of climate change over human interventions in shaping the hydrological characteristics of the lake.

Gocic and Trajkovic (2013) provides a comprehensive analysis of meteorological trends at twelve weather stations across Serbia from 1980 to 2010. Utilizing the non-parametric Mann-Kendall and Sen's slope methods, the research identifies both positive and negative trends in seven key meteorological variables. Seasonal and annual trends in minimum and maximum air temperatures show a clear upward trajectory, indicative of warming patterns. Meanwhile, relative humidity displays a significant decrease during the summer and autumn seasons. Vapor pressure trends upward in the spring, summer, and autumn, reflecting changes in atmospheric moisture content. Notably, precipitation

patterns do not exhibit significant trends in the summer and winter, suggesting variable rainfall over the study period. Cumulative sum charts and bootstrapping methods further validate these findings, marking abrupt changes and enhancing the robustness of trend detection. Overall, the study effectively highlights the dynamic nature of Serbia's climate over three decades, underscored by methodological rigor in trend analysis of meteorological data.

Yadav *et al.*,(2014) conducted a study focused on the quantitative estimation of rainfall and temperature trends, crucial for water resource management, flood forecasting, and climate change studies in Uttarakhand .Global Climate Models (GCMs) simulations predict an increase in extreme daily rainfall events globally and a decrease in overall regional rainfall due to greenhouse gas emissions .Previous studies have noted a decline in precipitation over the Himalayan region in the last two decades and significant inter-annual variations in extreme rainfall events across India .Uttarakhand, a state in the Indian Himalayas heavily reliant on agriculture, highlights the necessity of continuous rainfall studies for effective water resource planning and management .The research employs the Mann-Kendall trend test, a widely used non-parametric test, to identify significant trends in precipitation and temperature for the periods 1971-2011 and 1971-2007 in Uttarakhand .The study aims to analyze the changing trends of rainfall and temperature across all thirteen districts of Uttarakhand, utilizing daily rainfall data from 1971 to 2011 and temperature data from 1971 to 2007

Rahman and Dawood (2016) research evaluated the temperature trends in the eastern Hindu Kush region of north Pakistan using the Mann–Kendall trend model (MKTM) and Sen’s slope estimator (SSE). Data sourced from the Pakistan Meteorological Department for seven meteorological stations facilitated the investigation into climate change impacts on regional temperature patterns. The study identifies an increasing trend in mean maximum temperatures at Chitral, Dir, and Saidu Sharif stations, contrasting with decreasing trends in mean minimum temperatures at Saidu Sharif and Timergara stations. These trends suggest significant spatio-temporal variability in temperature, which is attributed to broader climate change influences affecting the region. The use of MKTM and SSE provides robust analytical frameworks to discern and quantify these trends, offering insights into the dynamic and complex interactions between climate change and regional meteorological patterns, thereby emphasizing the critical need for targeted climate adaptation strategies in the area.

Phuong *et al.*,(2020)study investigated hydro-meteorological trends in the Vu Gia Thu Bon watershed from 1979 to 2014. By combining the Innovative-Şen trend method with classical Mann-Kendall tests, the research identifies significant increasing trends in annual rainfall, extreme temperatures, relative humidity, and stream flow. Conversely, evapotranspiration and sunshine duration exhibit opposing trends. Notably, maximum and minimum temperature warming trends are 0.019°C/year and 0.024°C/year, respectively. The study underscores the applicability of the Innovative-Şen approach for trend identification. These findings have implications for climate-induced risks and water resource management in the study area during the climate emergency

Sa'adi *et al.*,(2023) in their study explored the spatio-temporal trends of extreme rainfall and temperature in Sarawak peatland over a 68-year period (1948–2016) using the Princeton gridded datasets and a Modified Mann-Kendall (MMK) test. This test enhances the standard Mann-Kendall (MK) method by addressing biases due to serial autocorrelation and scaling effects inherent in climate data, thus providing a more accurate trend analysis of extreme climate events influenced by large-scale climate phenomena. Their findings, processed through the R-based RCLimDex, indicated significant, albeit spatially varied, increases in extreme rainfall during the Southwest monsoon compared to the Northeast monsoon. Additionally, variations in diurnal temperature range were observed, with an expected decrease during both monsoons as minimum temperatures rose more sharply than maximum temperatures. The study highlights the critical impacts of extreme weather conditions on the peatland's dual role as a carbon sink and source, underlining the urgency of addressing climate change effects in this sensitive ecosystem.

Fattah *et al.*,(2024) investigates the variability and trends in rainfall patterns across South Asian capitals, examining their implications for groundwater resource management amid climate change and human activities. Utilizing Mann-Kendal tests, Innovative Trend Analysis, and Continuous Wavelet Coherence, the research identifies consistent trend patterns in rainfall across various timescales. The study employs Gumbel distribution for Intensity-Depth-Frequency(I-D-F) analysis to quantify rainfall depth and intensity over durations ranging from 5 minutes to 24 hours across multiple return periods. Results indicate significant spatial variability, with Kotte experiencing the highest annual rainfall and Kabul the least. Most cities show a positive annual rainfall trend, with monthly and seasonal variations. The findings highlight the potential impacts

of these trends on groundwater resources and are critical for developing strategies within the water-energy-food nexus, informing water policy, and addressing the social dimensions of water resource management in a changing climate.

2.3 DETECTION OF CHANGE POINT FOR THE METEOROLOGICAL VARIABLE TIME SERIES BY PETTIT TEST

Rougé *et al.*,(2013) addressed the challenge of detecting change point in hydrological time series, such as shifts in precipitation and streamflow, which are critical for water resources management. Authors critiqued traditional methods for their inability to distinguish between gradual and abrupt changes effectively. A novel method was proposed, combining the Mann–Kendall rank correlations with Pettitt statistics to identify the nature of shifts in hydro climatic data. Validated through Monte-Carlo simulations, this approach demonstrated robustness irrespective of data length. The method was applied to analyse hydroclimatic changes across the United States from 1910 to 2009, using data from 1217 USHCN stations.

Li *et al.*,(2014) examined change point detection in hydrological data consistency. Initially, the Pettitt test was used to detect change points for annual rainfall and runoff time series in six selected sub-watersheds of the Luanhe river basin in Northeast China. Subsequently, they introduced a method to detect change points based on the law of mutual change of quality and quantity in variable fuzzy sets. The mean of the time series served as the assessment index, similar to other change point detection methods. They defined the 95% and 5% quantiles of the time series as the supremum and infimum, respectively. A reference period (e.g., the first 10 points of the time series) was selected as the stationary period. After the reference period, they examined the mean value of the time series point by point. This method was applied to the six sub-watersheds of the Luanhe river basin. The results of the two methods indicated that most annual rainfall time series did not exhibit change points, while some annual runoff time series showed change points in 1979 or 1981. A comparison of the two methods revealed that the Pettitt test provided a reference for the variable fuzzy sets method, but the latter yielded more reasonable results than the Pettitt test in this study. Furthermore, this method can be applied to other natural time series.

Palaniswami and Muthiah (2018) conducted a study that focused on analysing the variability of rainfall and temperature to understand the hydrological environment in a

river basin in northern Tamil Nadu. Using Mann-Kendall and Sen's slope tests, the researchers examined temperature trends on monthly, seasonal, and annual scales, along with annual maximum daily rainfall and other rainfall metrics. Additionally, a change point detection test was conducted for annual maximum and minimum, mean temperatures, and annual precipitation series. The findings indicated significant rising trends in all evaluated temperature parameters across different time scales. Particularly notable were the more pronounced temperature increases during the north-east and south-west monsoons compared to the summer and winter seasons across various rain gauge stations. Change points in maximum and minimum temperatures were identified in specific years, confirming shifts in climate patterns. This comprehensive analysis sheds light on significant climatic changes within the region, emphasizing the need for targeted climate adaptation strategies.

Animashaun *et al.*,(2020) in their study investigated the spatio-temporal variability of rainfall across 33 sub-basins in the Niger Central Hydrological Area (NCHA), Nigeria, spanning 105 years (1911–2015). Utilizing CRU data (CRU_TS 4.01), they employed rainfall variability indices, precipitation concentration indices, and linear regression models (LRMs). Change point detection using nonparametric Mann-Kendall (MK) tests, Standard Normal Homogeneity Test (NSHT), and Pettitt's test (PT) revealed significant trends. The wettest and driest years were 1983 and 1911, respectively, while the wettest and driest decades were 1921–1930 and 1981–1990. LRM indicated decreasing mean annual rainfall, early rainy season, and main rainy season. NSHT and PT identified 1969 as the probable change point.

Getahun *et al.*,(2021) examined climatic trends and change-points in the Awash river basin (ARB) from 1986 to 2016, utilizing data from 29 meteorological stations. It applied Pettitt's, the von Neumann ratio (VNR), Buishand's range (BR), and standard normal homogeneity (SNH) tests for change-point detection, alongside the Mann-Kendall (MK) test for trend analysis on rainfall and temperature. The research revealed significant increasing trends in both annual and seasonal temperatures, with notable temperature change-points identified in 2001 for the annual and major rainy seasons, and 1997 for the minor rainy season. Conversely, rainfall showed a significant decreasing trend, particularly in the downstream parts of the ARB, with a shift and high variability linked to El Niño and La Niña events. The mRS rainfall exhibited a change-point in 1998, followed by a mean annual decrease of 52.5 mm. The study underscored the critical need

for integrated water management and early detection of El Niño events to mitigate potential negative impacts on the basin's agriculture-dependent communities.

Kumar *et al.*,(2023) , conducted research in the Garo Hills region of Northeast India, analysed climatic changes and their impacts on forest cover loss and CO₂ emissions from 1984 to 2019. Using secondary data, the study employed Mann-Kendall's and Sen's slope tests to assess trends in climatic parameters such as precipitation, temperatures, and relative humidity, while Pettitt's test identified change points. The findings revealed a general decrease in precipitation and an increase in maximum temperatures across most time frames. Minimum temperatures showed a decreasing trend, and relative humidity increased in all seasons except the monsoon. The study also explored correlations between these climatic factors and environmental changes using Pearson's correlation and regression analysis. It found significant positive correlations between maximum temperature and both forest cover loss and CO₂ emissions, while minimum temperature had negative correlations with these variables. These insights are crucial for developing targeted climate adaptation and mitigation strategies in the region.

2.4 TIME SERIES ANALYSIS OF METEOROLOGICAL VARIABLES USING WAVELET COHERENCE

Araghi *et al.*,(2016) explored the relationships between precipitation in Iran and three major climatic teleconnection indices—Arctic Oscillation (AO), North Atlantic Oscillation (NAO), and Southern Oscillation Index (SOI)—over the period from 1960 to 2014. Utilizing wavelet coherence (WCO) at 30 synoptic stations, the research identified that SOI had the strongest influence on precipitation patterns across Iran, while AO and NAO also exhibited significant effects. The findings highlighted the dominant period of influence for AO at most stations as being 32 months or more, whereas for NAO, it extended to 64 months or more. SOI impacted most of the country on a shorter scale of less than 64 months, except in the north-western regions where its influence lasted longer. The phase relationships between these indices and precipitation varied, often showing random patterns, with long-term SOI showing an anti-phase relationship at many stations. The study underscored the effectiveness of WCO as a method for analyzing time-frequency relationships in climatic and hydrological studies.

Bonkaney *et al.*,(2019) employed Wavelet Transform Coherence (WTC) and phase analysis to investigate the relationship between daily electricity demand (DED) and

various weather variables, including temperature, relative humidity, wind speed, and radiation. The analysis revealed that while DED exhibited both seasonal fluctuations and an upward trend, the weather variables mainly showed seasonal variations. The application of WTC and phase analysis enabled the identification of periods where significant correlations existed between DED and specific weather variables. Notably, a strong seasonal interdependence was found between air temperature and DED within 256-512 days and 128-256 days periods. A significant correlation was also observed between humidity and DED within a 256-512 day period, achieving an average coherence of 0.8. However, correlations between DED and both radiation and wind speed were weak, with average coherence values below 0.5. These findings provide valuable insights for power planners to enhance forecasting and planning of electricity demand based on weather conditions.

Li *et al.*,(2019) conducted study in a karst depression in south-west China, researchers investigated the relationships between temporal soil water content (SWC) and meteorological factors over a period of 242 days. Utilizing time domain reflectometry, SWC was measured at five different soil depths across two types of land use: farmland and grassland. The study employed wavelet coherency analysis to assess the scale-dependent influences on SWC, recognizing that traditional Pearson's correlation analysis might not capture these complex relationships effectively. The results highlighted that precipitation and land use were the primary drivers of SWC dynamics, with distinct patterns observed between farmland and grassland. Wavelet coherency analysis revealed both positive and negative correlations between SWC and meteorological factors, varying significantly across scales. This approach also demonstrated that soil depth influenced SWC dynamics more prominently at larger scales compared to land use. The study underscored the potential of wavelet coherency analysis to enhance soil moisture prediction by identifying scale-specific dependencies.

Nourani *et al.*,(2019) work explored the influence of hydro-climatological variables on water level fluctuations in Urmia Lake in Iran and Van Lake in Turkey, employing wavelet transform coherence (WTC) to analyze the complex interactions. The study focused on the hydrological time series' higher order moments to understand the complexity and variability of water levels in these two geographically proximate yet ecologically distinct saline lakes. The analysis revealed that runoff exhibited the strongest coherency with water level fluctuations, achieving coherence values between 0.9 and 1.0.

Despite similar climatic conditions, Urmia Lake displayed a concerning negative trend in water levels over the past 15 years, highlighting its critical ecological status. The research emphasized the importance of local multi-scale correlations and phase relationships, offering insights into how these lakes respond to varying hydroclimatological inputs. This comparison not only pinpointed the critical conditions of Urmia Lake but also underscored the need for regional water management strategies to mitigate adverse trends.

Das *et al.*,(2020) in their study, analysed the relationships between monthly precipitation patterns in six meteorologically homogeneous regions of India and eight large-scale climatic oscillations from 1951 to 2015. The climatic indices examined included the Indian Ocean Dipole (IOD), Sea Surface Temperature (SST), Multivariate ENSO Index (MEI), Southern Oscillation Index (SOI), Pacific Decadal Oscillation (PDO), North Atlantic Oscillation (NAO), Arctic Oscillation (AO), and the Indian Summer Monsoon Index (ISMI). Utilizing wavelet and global coherence analyses, the study found that while all climatic indices significantly affected precipitation, ISMI had the most pronounced impact, especially on an intra-annual scale across Central Northeast, Peninsular, and West Central India. The effective period for IOD spanned 8 to 16 months, and for ENSO-related indices like SST, SOI, and MEI, it was between 20 and 54 months. The study demonstrated the efficacy of wavelet and global coherence methods in revealing complex, scale-specific relationships between large-scale climatic oscillations and regional precipitation, offering valuable insights for water resource management and hydrological forecasting.

Zhou *et al.*,(2022) analysed in the Pearl river basin, long-term data on the Normalized Difference Vegetation Index (NDVI) and Solar-induced chlorophyll fluorescence (SIF) to understand how vegetation dynamics respond to meteorological drought. From 2001 to 2019, vegetation showed an increasing trend, with SIF gains outpacing NDVI. Vegetation response times varied between indices and vegetation types, being quicker in woody savannas and slower in evergreen broadleaf forests. The study revealed stronger correlations between SIF and drought than NDVI. Large-scale climate oscillations such as ENSO, PDO, and sunspot activities were identified as significant drivers of these interactions, with PDO having the most pronounced impact.

Materials and methods

CHAPTER III

MATERIALS AND METHODS

In this study, three climatic variables (precipitation, max and minimum temperature) were considered for the analysis. Future projected climatic variables were collected from 13 different CMIP6 climatic models under four SSPs scenarios: two are from (SSP1–2.6 and SSP5–8.5 Wm^{-2}), one from pessimistic (SSP3–7.0 Wm^{-2}) and one based on historical trend (SSP2–4.5 Wm^{-2}). Trend analysis was done using Modified Mann Kendall test and Sen’s slope test. Change point detection was done using the Pettit test and the dependence of the meteorological variables between each other was analysed using the wavelet coherence plot.

3.1 STUDY AREA DESCRIPTION

India is situated north of the equator between $8^{\circ}4'$ north (the mainland) to $37^{\circ}6'$ north latitude and $68^{\circ}7'$ east to $97^{\circ}25'$ east longitude. It is the seventh-largest country in the world, with a total area of 3,287,263 square kilometres (1,269,219 sq mi). India accounts 2.42% of the total world land area. In the 21st century, the global environment faces significant threats due to climate change, ranging from floods and droughts to heat waves and other extreme weather events. In recent decades, India has experienced severe flooding and prolonged droughts, compounding challenges related to livelihoods, public health, and population displacement. The availability of precise and robust climate change information is paramount in addressing and mitigating the adverse impacts on a region's environment and its communities.

According to Singh (2024), Koppen’s classification is based on the empirical relationship between climate and vegetation. The classification provides an efficient way to describe climatic conditions defined by precipitation and temperature and their seasonality. The classification is widely used to map long term climate and associated ecological conditions. If data on temperature, precipitation and seasonality is available, it is easy to code the climate type. Selected cities with their corresponding Koppen climatic zones are enlisted in table 3.1

Table 3.1 List of selected cities with their corresponding Koppen climatic zone

Climate Area	Type	Location
Amw	Monsoon with a short dry season	The west coast of India south of Goa
As	Monsoon with dry summer	Coromandel coast of Tamil Nadu
Aw	Tropical savannah	Most of the Peninsular plateaus, south of the Tropic of Cancer
BShw	Semi-arid steppe climate	North-western Gujarat, some parts of western Rajasthan, and Punjab
BWhw	Hot Desert	Extreme western Rajasthan
Cwg	Monsoon with dry winter	Ganga Plain, eastern Rajasthan, northern Madhya Pradesh, most of North-east India
Dfc	Cold humid winter with short summer	Arunachal Pradesh
E	Polar type	Jammu and Kashmir, Himachal Pradesh, and Uttarakhand

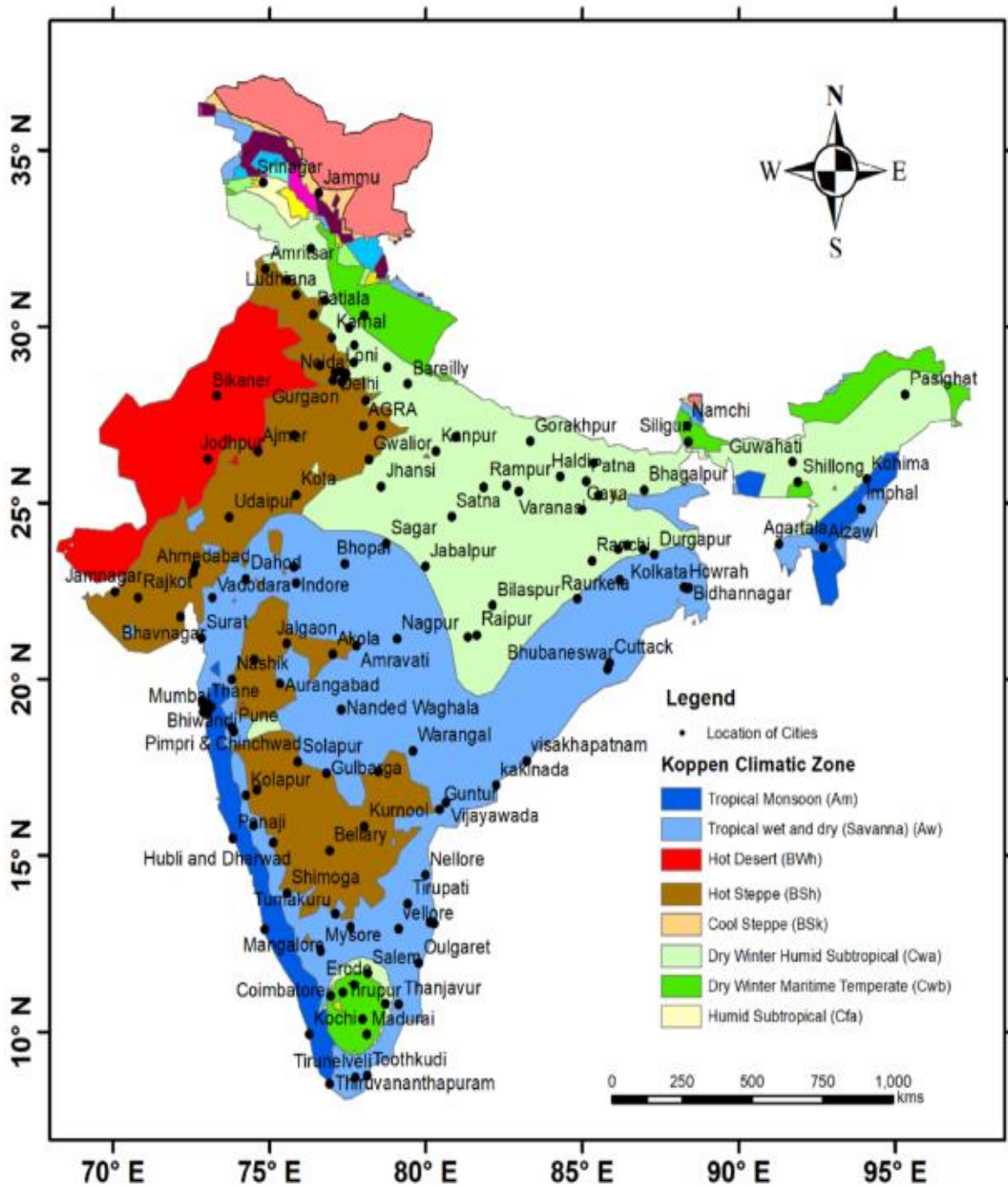


Fig. 3.1 Koppen's climatic classification -India

3.2 DATA COLLECTION AND SOFTWARE USED

In this study, three climatic variables (precipitation, max and minimum temperature) were considered for the analysis. Future projected climatic variables are collected from 13 different CMIP6 climatic model (Table 1) under four SSPs scenarios: two are from optimistic (SSP1–2.6 and SSP5–8.5 Wm⁻²), one from pessimistic (SSP3–7.0 Wm⁻²) and one based on historical trend (SSP2–4.5 Wm⁻²). Three climatic variables at daily timescale and 0.25° × 0.25° fine spatial resolution in bias corrected format is downloaded from zenodo platform (Mishra *et al.*, 2020). Data source with spatial resolution and timespan are enlisted in the table 3.2

Table 3.2 Data source with spatial resolution and timespan

DATA	SOURCE	TIMESPAN	SPATIAL RESOLUTION
Historic precipitation	IMD,Pune	1951-2022	0.25° × 0.25°
Historic maximum temperature	IMD,Pune	1951-2022	1° × 1°
Historic minimum temperature	IMD,Pune	1951-2022	1° × 1°
Future precipitation	Mishra <i>et al.</i> , 2020 (Zenodo)	2024-2100	0.25° × 0.25°
Future maximum temperature	Mishra <i>et al.</i> , 2020 (Zenodo)	2024-2100	0.25° × 0.25°
Future minimum temperature	Mishra <i>et al.</i> , 2020 (Zenodo)	2024-2100	0.25° × 0.25°

Besides, for the historic climatic variable analysis, observed historical daily rainfall data (1950–2022) at 0.25° × 0.25° spatial resolution, maximum and minimum temperature at 1° × 1° at spatial resolution at daily timescale obtained from the India Meteorological Department (IMD), Pune ([https:// imdpu ne. gov. in/ Clim_ Pred_ LRF_ New/ Grided_ Data_ Download. html](https://imdpu ne. gov. in/ Clim_ Pred_ LRF_ New/ Grided_ Data_ Download. html)) were considered. To have uniform grid point for effective spatial analysis, the past observed grid data was regridded for future grid point

of CMIP6 model, using Inverse Distance Weightage (IDW) spatial interpolation technique, one of the effective re gridding method (Das et al., 2016).

Regarding individual model concern, there is uncertainty and discrepancies in model performance, which can be attributed to the variations in dataset preparation and their resolution (Saharwardi and Kumar, 2021). To reduce uncertainty in individual model and to have reliable climatic projection, ensemble approach was used for the 13 CMIP6 models, that ensemble approach has shown good performance over individual model as reported by earlier researchers (Knutti et al., 2010; Ahmed et al., 2019 and Saharwardi and Kumar, 2021). CMIP6 models used in this study along with country of origin and spatial resolution are provided in table 3.2

Table 3.3 List of CMIP6 models used in this study along with country of origin

No	Models	Spatial resolution Longitude x Latitude	Country
1.	ACCESS-CM2	1.9° x 1.3°	Australia
2.	ACCESS-ESM1-5	1.9° x 1.2°	Australia
3.	BCC-CSM2-MR	1.1° x 1.1°	China
4.	CanESM5	2.8° x 2.8°	Canada
5.	EC-Earth3	0.7° x 0.7°	Europe
6.	EC-Earth3-Veg	0.7° x 0.7°	Europe
7.	INM-CM4-8	2° x 1.5°	Russia
8.	INM-CM5-0	2° x 1.5°	Russia
9.	MPI-ESM1-2-HR	0.9° x 0.9°	Germany
10.	MPI-ESM1-2-LR	1.9° x 1.9°	Germany
11.	MRI-ESM2-0	1.1° x 1.1°	Japan
12.	NorESM2-LM	2.5° x 1.9°	Norway
13.	NorESM2-MM	2.5° x 1.9°	Norway

The softwares used for the study are enlisted below ;

- a. ArcGIS - The results of trend analysis and the change point analysis was projected as maps in ArcGIS (Shown in figure 3.2)
- b. MATLAB - The complete study was done by running the codes in MATLAB (Shown in figure 3.3)



Fig. 3.2 ArcGIS



Fig. 3.3 MATLAB

3.3 IDENTIFICATION OF SUITABLE CLIMATIC MODEL

The most suitable climatic model after the ensembled data for the eight Koppen's climatic regions was identified through this objective. Flow chart showing the procedure for the Identification of suitable climatic model is shown in figure 3.4.

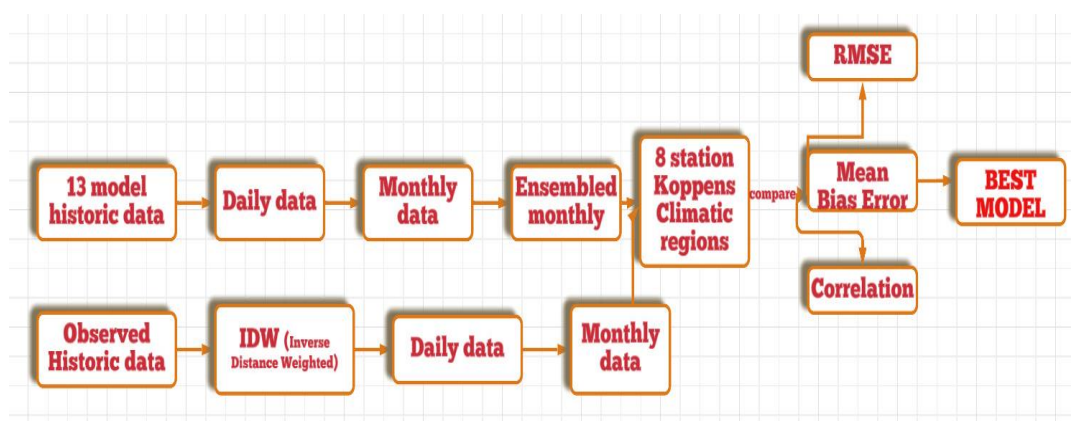


Fig. 3.4 Flow chart for the Identification of suitable climatic model

Conversion of past daily data to monthly data was done separately for all the 13 models and then the ensembled monthly data was computed. According to the Koppen climatic classification, points corresponding to the selected 8 stations were selected for 13 models as well as the ensembled data and Correlation, Root Mean Square Error (RMSE) and Mean Bias Error were computed.

Precipitation daily raw data of 4641 stations of 13 climatic model was taken from a time period of 1951 to 2014. The daily raw data was converted into monthly data using MATLAB. Past original data of monthly precipitation from time period of 1951 to 2014 was also taken. An excel sheet was created consisting of data from eight Koppen climatic classified stations of each climatic model from the monthly data of models. Another excel sheet was also created consisting of data only taken from Koppen's climatic regions out of 4641 stations from monthly historic data. Ensembled monthly was obtained from the above 13 models data. Another excel was created for comparing the past original precipitation data with the past precipitation data of 13 models as well as ensembled data. Comparison was done mainly using Correlation coefficient, Root mean square error (RMSE) and Mean bias error which are obtained using MATLAB. For each

station 13 models as well as ensembled data's correlation coefficient, RMSE, mean bias error value were obtained and by comparing these values the best model suited for each station was found out . Also the relevance of using ensembled data compared with the 13 models data was understood.

3.3.1 Analysis of performance to identify the best model

3.3.1.1 Correlation coefficient

Correlation coefficient (a value between negative1 and positive1) tells how strongly two variables are related to each other. A correlation coefficient of positive1 indicates a perfect positive correlation. As variable x increases, variable y increases. As variable x decreases, variable y decreases. A correlation coefficient of negative1 indicates a perfect negative correlation. As variable x increases, variable z decreases. As variable x decreases, variable z increases. A correlation coefficient near 0 indicates no correlation.

$$r = \frac{n(\sum xy) - (\sum x)(\sum y)}{\sqrt{[n \sum x^2 - (\sum x)^2][n \sum y^2 - (\sum y)^2]}}$$

Where r is the Correlation coefficient, n is the number in the given dataset, x,y will be first and second variable in the context.

3.3.1.2 Root mean square error (RMSE)

Root mean square error (RMSE) is a metric that tells us the average distance between the predicted values from the model and the actual values in the dataset. The lower the RMSE, the better a given model is able to fit a dataset.

$$RMSE = \sqrt{\frac{\sum_{i=1}^n (X_{obs,i} - X_{model,i})^2}{2}}$$

Where $X_{(obs,i)}$ is the observation value and $X_{(model,i)}$ is the forecast value. n is the number of observations.

3.3.1.3 Mean bias error

Mean bias error can be simply estimated as the difference between the means of predictions and observations. The closer to zero the better. Negative values indicate underestimation. Positive values indicate general overestimation.

$$MBE = \frac{1}{n} \sum_{i=1}^n (P_i - O_i)$$

Where O_i is the observation value and P_i is the forecast value.

Correlation coefficient was computed using Microsoft Excel whereas the RMSE and the Mean bias error were computed using the Agrimetsoft application.

3.4 TREND ANALYSIS OF METEOROLOGICAL VARIABLES USING MODIFIED MANN-KENDALL AND SEN'S SLOPE TEST FOR THE INDIA

Using MMK and Sen's Slope tests, trends in the historic as well as future meteorological data were analysed. Flow chart showing the procedure for the trend analysis of meteorological variables is shown in figure 3.5.

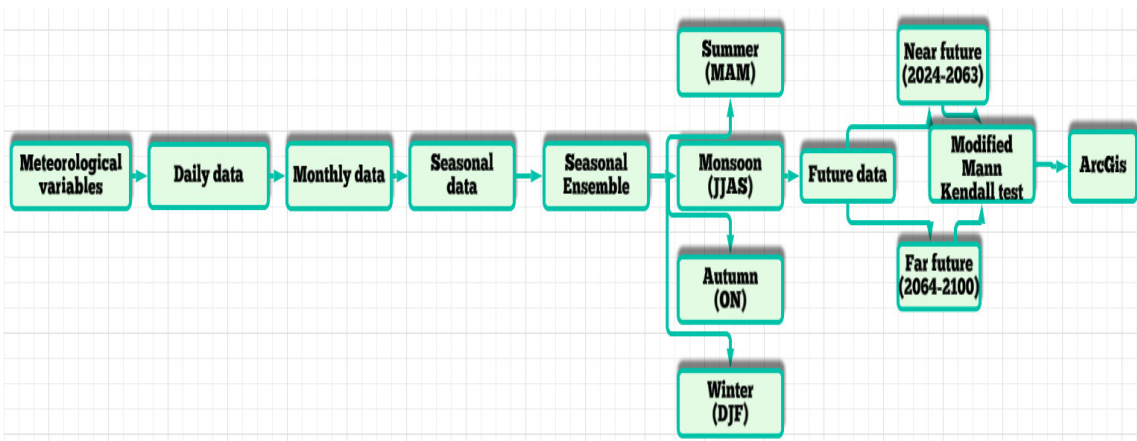


Fig. 3.5 Flow chart for the trend analysis of meteorological variables

After the conversion of daily data to monthly data and then to the seasonal data, the ensembled seasonal averages were computed for the nominal seasons winter (i.e., December–January– February), summer (March–April–May), monsoon (June–July– August–September) and autumn (October–November) for the 13 models. The dataset was

then grouped as near (2024- 2060) and far future (2061- 2100). Using the MATLAB codes, MMK and SSE tests were done for all the 4 SSP scenarios and then the z values (MMK) and the Sen's slope values were projected in ArcGIS.

3.4.1 Analysis of trends using MMK and SSE

To study the trend of meteorological variables, non-parametric trend analysis tests such as Modified Mann–Kendall (MMK) test and Theil–Sen's slope estimator was used in this study. Hamed and Rao (1998) developed MMK after doing variance correction in the traditional MK test that was originally developed by Mann (1945) and Kendall (1975) to address the problem of autocorrelation in the time series data. MK used to detect the presence of a monotonic trend in a time series dataset. MMK detects the presence of trend. Sen's slope test was used to quantify trends in terms of numerical value. This numerical value helps in quantifying and understanding the trend present in the data, whether it's increasing, decreasing, or remaining stable over time. Code used to run SSE was provided in appendix II.

The Mann–Kendall test statistics S is calculated using the formula given as

$$S = \sum_{i=1}^{N-1} \sum_{j=i+1}^N \text{sgn}(x_j - x_i)$$

where x_j and x_i are the annual data values in year j and i , respectively, $j > i$ and N is the number of data points.

Modified Mann–Kendall test Significant values of ρ_k have only been used calculating the variance correlation factor n/n_s^* , as the variance of S is underestimated for the positively autocorrelated data:

$$\frac{n}{n_s^*} = 1 + \frac{2}{n(n-1)(n-2)} \times \sum_{k=1}^{n-1} (n-k)(n-k-1)(n-k-2)\rho_k$$

where n represents the actual number of observations, n_s^* is represented as an effective number of observations to account for the autocorrelation in the data and ρ_k is considered as an autocorrelation function of the ranks of the observations.

The N values of Q_i are ranked from smallest to largest and the median of slope or Sen's slope estimator is computed as:

$$Q_{med} = \begin{cases} Q_{\left[\frac{(N+1)}{2}\right]}, & \text{if N is odd} \\ \frac{Q_{[N/2]} + Q_{[(N+2)/2]}}{2}, & \text{if N is even} \end{cases}$$

3.5 IDENTIFICATION OF CHANGE POINT IN UPCOMING TIME PERIOD FOR THE METEOROLOGICAL VARIABLES

After the conversion of daily data to monthly data and then to the seasonal data, ensembled seasonal averages were calculated for the nominal seasons winter (i.e., December–January– February), summer (March–April–May), monsoon (June–July– August–September) and autumn (October–November) of 13 models. Using the MATLAB codes, Pettit test was done for all the 4 SSP scenarios and then the change points were projected in ArcGis. Flow chart showing the procedure for the identification of change point in upcoming time period for the meteorological variables are shown in figure 3.6.

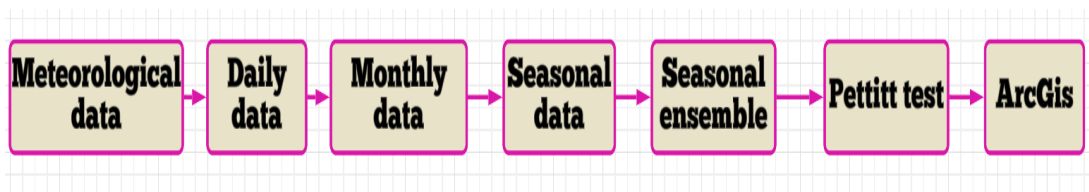


Fig. 3.6 Flow chart for the identification of change point in upcoming time

The Pettit change point test is a non-parametric statistical test that can be used to identify a single change point in a time series. It is essential in the analysis of climate and hydrological data to detect a shift or an abrupt change. According to Smadi and Zghoul(2005) test was formulated by Pettit and can be written as follows:

$$U_k = 2 \sum_{i=1}^k M_i - k(n + 1)$$

where M_i is the rank of the i -th observation when the values X_1, X_2, \dots, X_n in the series are arranged in ascending order. Code used to run pettit test was provided in appendix II

3.6 COMPARISON OF FUTURE TIME SERIES OF METEOROLOGICAL VARIABLES USING WAVELET COHERENCE

The wavelet coherence plot is a valuable technique for investigating the correlation between two signals in both time and meteorological parameters. It provides insights into the dynamic relationships between signals, revealing areas of strong correlation or no correlation. Wavelet coherence is useful for analyzing nonstationary signals. The authors intend to observe how correlations vary over certain frequencies and time intervals through wavelet coherence. The wavelet coherence plot brings out a figure with time on the x-axis and frequency of period value on the y-axis. The lower frequency values give higher scale values or periods of co-movement. On the right-hand side, the bar indicates the power of the coherence. The yellow colour means higher power, and the blue colour means lower coherence between the terms. The thin, faded section around the edges indicates the cone of influence area. It is due to the low efficiency of the results obtained by the wavelet transform at the edges of the time series data. The areas that are contoured with black lines indicate a 5% significance level against noise. The blue regions represent no time or frequency dependence at the 5% significance level. The arrows indicate the relationship between two time series in phase. Arrows pointing to the right mean positive dependence, and arrows pointing to the left mean a negative relationship. If the arrow is pointing up, the first series is leading the second in the analysis, and the down-pointing arrows indicate the second series as the leading item in that time and frequency region. Here, the horizontal axis and the vertical axis represent frequency in days and time, respectively. Wavelet coherence is a measure of the correlation between two signals. The wavelet coherence of two time series x and y is:

$$\frac{|S(C_x(a, b)C_y^*(a, b))|^2}{S(|C_x(a, b)|^2).S(|C_y(a, b)|^2)}$$

where $C_x(a, b)$ and $C_y(a, b)$ denote the continuous wavelet transforms of x and y at scales a and positions b . The superscript $*$ is the complex conjugate and S is a smoothing operator in time and scale.

For real-valued time series, the wavelet coherence is real valued if you use a real-valued analyzing wavelet, and complex valued if you use a complex-valued analyzing wavelet.

Flow chart showing the procedure for the comparison of future time series of meteorological variables using wavelet coherence is shown in figure 3.7.

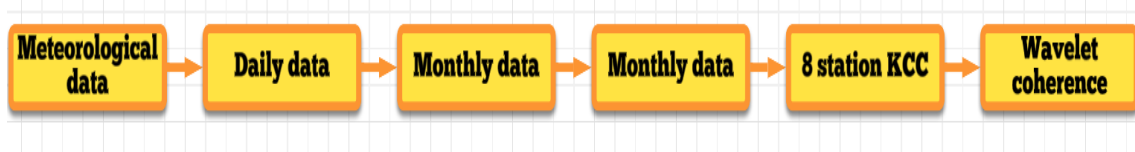


Fig. 3.7 Flow chart for the comparison of future time series of meteorological variables using wavelet coherence

After the conversion of daily data to monthly data and then ensemble monthly averages of 13 models were calculated. The data corresponding to the 8 climatic regions according to the Koppen's climatic classification was extracted. Using the MATLAB codes, wavelet coherence plots were generated for all the 4 SSP scenarios.

Historical (1951- 2022) and Future (2024- 2100) data of three meteorological variables (Precipitation, Maximum temperature and Minimum temperature) as per the the 13 Global Climatic Models (GCMs) under the CMIP6 were analysed using MMK, Sen's slope test (trend) and the Petit test (change point analysis). Considering the Koppen's climatic classification, most suitable model as well as the correlation between temperature and precipitation (Wavelet coherence) were also investigated.

Results and discussion

CHAPTER IV

RESULTS AND DISCUSSION

The results of identification of suitable climatic model, trend analysis as well as the correlation plots are presented in this chapter.

4.1 IDENTIFICATION OF SUITABLE CLIMATIC MODEL

Suitable climatic model for each region was identified on the basis of values of correlation coefficient, root mean square error and mean bias error. In the comparison of 13 models as well as the ensembled data among eight stations, ensemble data is found to be the best. Correlation coefficient of positive 1 indicates a perfect positive correlation and negative 1 indicates a perfect negative correlation. The lower the RMSE, the better a given model is able to fit a dataset. Mean bias error can be simply estimated as the difference between the means of predictions and observations. The closer the mean bias error to zero the better is the model. Negative values indicate underestimation. Positive values indicate general overestimation. Result of the model analysis for the region Amw is given in the table 4.1. Similar tables corresponding to the remaining seven regions are given in appendix I.

Table 4.1 Result of the model analysis for the region Amw

MODELS	Amw		
	CORRELATION COEFFICIENT	RMSE	MEAN BIAS ERROR
ACCESS-CM2	.22	10.98	-2.24
ACCESS-ESM1-5	.66	11.30	-2.22
BCC-CSM2-MR	.81	8.08	-2.20
CanESM5	.62	10.97	-2.23
EC-Earth3	.67	10.68	-2.203
EC-Earth3-Veg	.69	10.27	-2.21
INM-CM4-8	.71	9.75	-2.19

INM-CM5-0	.73	9.58	-2.22
MPI-ESM1-2-HR	.68	10.03	-2.21
MPI-ESM1-2-LR	.78	8.56	-2.19
MRI-ESM2-0	.62	11.46	-2.26
NorESM2-LM	.74	9.34	-2.22
NorESM2-MM	.77	8.88	-2.18
ENSEMBLE	.84	7.76	-2.21

Table 4.2 Suitable model for different climatic regions

STATION	BEST MODEL
Amw-Maharashtra	BCC-CSM2-MR
As-Tamilnadu	ACCESS-CM2
Aw-Madhya Pradesh	MPI-ESM1-2-LR
Bshw-Rajasthan	BCC-CSM2-MR
Bwhw- Extreme Western Rajasthan	MPI-ESM1-2-LR
Cwg- Uttar Pradesh	EC-Earth3
Dfc-Arunachal Pradesh	EC-Earth3-Veg
E-Himachal Pradesh	EC-Earth3-Veg

In the first region Amw(Maharashtra) BCC-CSM2-MR model turn out to be the best comparing with other models . BCC-CSM2-MR model RMSE value is 8.08 which is the lowest value among rest,correlation value is .81 shows the highest positive correlation,mean bias error is -2.02. Table 4.2 shows the suitable model for different climatic regions.

In the second region As(Tamilnadu) ACCESS-CM2 model is best and its RMSE value is 4.45 which is the lowest value among rest, Correlation value is .51 shows the highest positive correlation, mean bias error is -0.01 lies near to the zero indicates it has less difference from original data.

In the Third region Aw(Madhya Pradesh) MPI-ESM1-2-LR model is best and its RMSE value is 4.57 which is the lowest value among rest, Correlation value is .68 shows the highest positive correlation, mean bias error is .10.

In the fourth region Bshw(Rajasthan) BCC-CSM2-MR model is best and its RMSE value is 2.69 which is the lowest value among rest, Correlation value is .38 shows the highest positive correlation, mean bias error is .063.

In the fifth region Bwhw(Extreme Westen Rajasthan) MPI-ESM1-2-LR model is best and its RMSE value is 2.01 which is the lowest value among rest, Correlation value is .20 shows the highest positive correlation, mean bias error is -0.01.

In the sixth region Cwg(Uttar Pradesh) EC-Earth3 model is best and its RMSE value is 4.25 which is the lowest value among rest, Correlation value is .69 shows the highest positive correlation, mean bias error is .38

In the seventh region Dfc (Arunanchal pradesh) EC-Earth3-Veg model is best and its RMSE value is 7.61 which is the lowest value among rest, Correlation value is .69 shows the highest positive correlation, mean bias error is -.55.

In the eighth region E (Himachal Pradesh) EC-Earth3-Veg model is best and its RMSE value is 3.27 ,Correlation value is .11 shows the positive correlation, mean bias error is .64, by comparing the rest models RMSE, mean bias error, correlation values.

4.2 ANALYSIS OF TREND OF METEOROLOGICAL VARIABLES WITH MMK AND SEN'S SLOPE TEST

Analysis of trends was done with MMK and sen's slope test .Trends in precipitation and temperature for entire India under four SSP scenarios for the time period 2024–2100 was analysed and the results are shown in table 4.4.

Table 4.3 Trends in precipitation and temperature for entire India under four SSP scenarios for the time period 2024–2100

PRECIPITATION			HISTORIC	SSP1 26	SSP2 45	SSP3 70	SSP5 86
	SUMMER	Z-Value	0.92	0.21	0.43	0.68	0.90
		Sen slope	0.002	0.001	0.003	0.005	0.006

	MONSOON	Z-Value	-0.06	0.43	0.75	1.22	1.93	
		Senslope	-0.0003	0.0083	0.0161	0.0271	0.0413	
	AUTUMN	Z-Value	-0.61	0.36	1.07	1.08	1.54	
		Senslope	-0.0017	0.005	0.009	0.013	0.023	
	WINTER	Z-Value	-0.03	0.06	-0.13	0.36	0.11	
		Senslope	0.0002	0.0003	-0.0004	0.0030	0.0008	
TMAX	SUMMER	Z-Value	1.108	1.559	4.007	5.953	6.737	
		Senslope	0.006	0.008	0.022	0.037	0.050	
	MONSOON	Z-Value	1.15	1.34	1.06	5.21	5.84	
		Senslope	0.0051	0.0076	0.0258	0.0329	0.0413	
	AUTUMN	Z-Value	2.79	1.57	3.33	5.63	6.47	
		Senslope	0.013	0.010	0.017	0.032	0.043	
	WINTER	Z-Value	1.49	2.39	4.36	5.56	6.51	
		Senslope	0.008	0.015	0.026	0.038	0.052	
	TMIN	SUMMER	Z-Value	1.49	1.71	5.24	7.05	7.65
			Senslope	0.003	0.008	0.025	0.045	0.055
MONSOON		Z-Value	1.05	1.77	5.52	7.14	7.58	
		Senslope	0.004	0.006	0.020	0.037	0.043	

	AUTUMN	Z-Value	2.57	1.27	5.04	6.92	7.37
		Sen slope	0.013	0.007	0.026	0.048	0.053
	WINTER	Z-Value	1.49	1.59	4.88	6.56	7.04
		Sen slope	0.010	0.011	0.030	0.053	0.062

Precipitation for the last seven decades has shown decreasing trend season to season for year wise except summer. Monsoon precipitation averagely decreased at the rate of -0.0003 mm per season for India. Maximum and minimum temperature increased for all the seasons. Particularly, summer season saw 0.006°C hike each season since mid of the 20th century. For the future time period, precipitation and temperature projected increasing pattern from SSP126 to SSP 586 case. Future monsoon under SSP126 case projected 0.0083 mm rainfall increase for each season, while SSP 586 shows 0.0413 mm per season. Projected summer also appears to be hottest as per SSP 586 case with 0.050°C temperature increase. In the eco-friendly SSP26 scenario, the temperature increase is in the modest level (0.008°C). Like rainfall increase, the variability of rainfall is also more in SSP 586 scenario. Spatially, western region projected more prone to high rainfall variability as well as rainfall decrease.

4.2.1 Precipitation

In order to analyse the trend of precipitation and temperatures for past as well as future under four SSP scenarios for four climatic seasons (summer, monsoon, autumn and winter), the MMK and Sen's slope test was applied.

4.2.1.1 Historical data

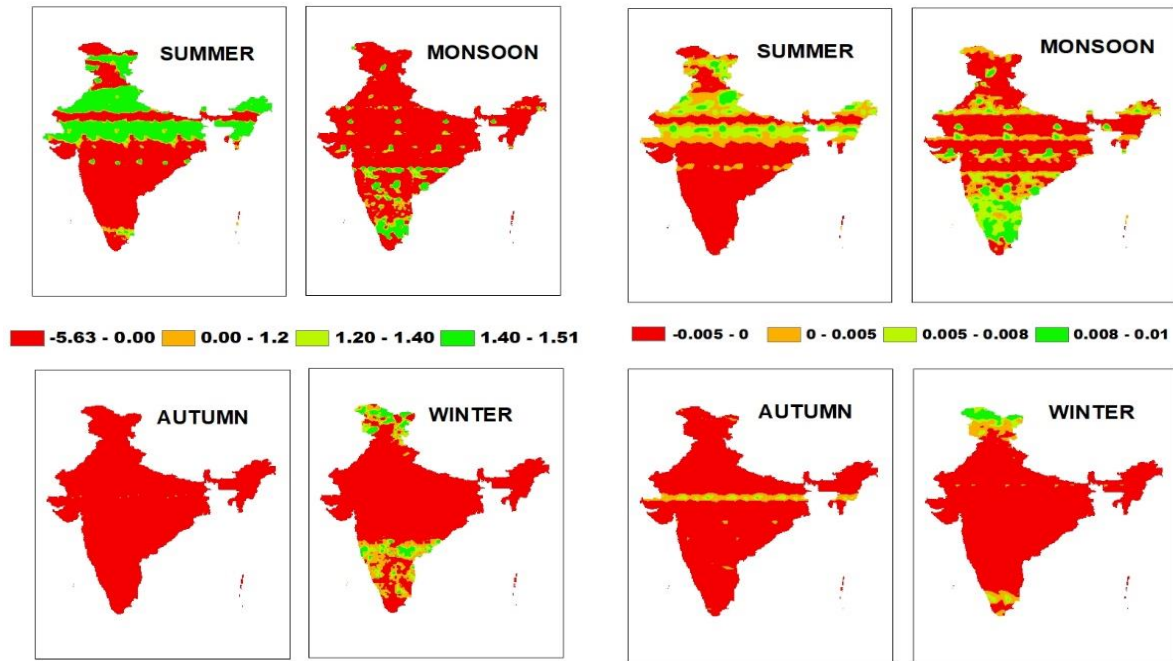


Fig. 4.1 Z value for trend analysis using historic data

Fig. 4.2 Sen's slope value for trend analysis using historic data

Z value for trend analysis using historic data is shown in figure 4.1. Sen's slope value for trend analysis using historic data is shown in figure 4.2. Overall, the historical trend of precipitation for the past seventy years since 1950 upto recent 2022 shows highly decreasing trend as per Z and Sen's slope value with minor exception for few regions. Regarding season and region specific, during summer season the Northern plain showed increasing trend, but in the case of monsoon season observed increasing trend for Southern region. For the autumn season whole of the country showed decreasing trend, while Himalayan region witnessed increasing winter rainfall as an exception one

The precipitation during the summer season is more in certain parts of Northern and central India, whereas it is almost uniform during monsoon season, very less or absent during autumn and the northern most parts receive more precipitation during the winters.

4.2.1.2 Future data-SSP 1

The future precipitation trend approached under near (2024-2060) and far future (2061-2100) time period. In the eco-friendly SSP scenario, despite not remarkable increasing trend, positive trend is observed for all the four seasons as well as most of the

country. Sen's slope value shows increasing trend of rainfall for all four seasons throughout the country. As far as time period is concerned, the near future shows relatively more increasing trend than far future. SSP1 near future Z value is shown in figure 4.3. SSP1 far future Z value is shown in figure 4.4.

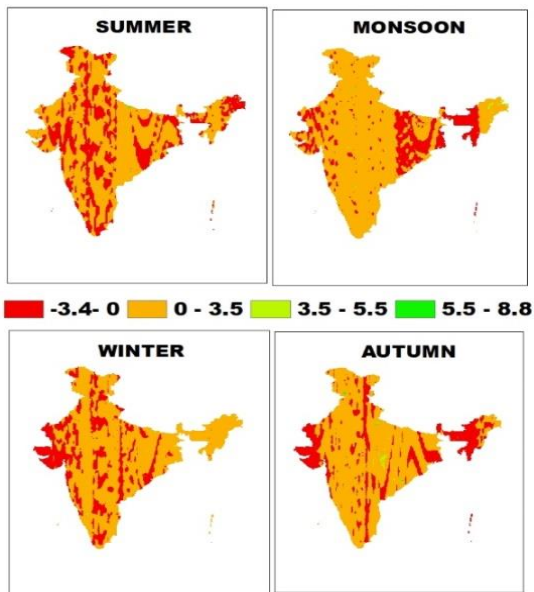


Fig. 4.3 SSP1 near future Z value

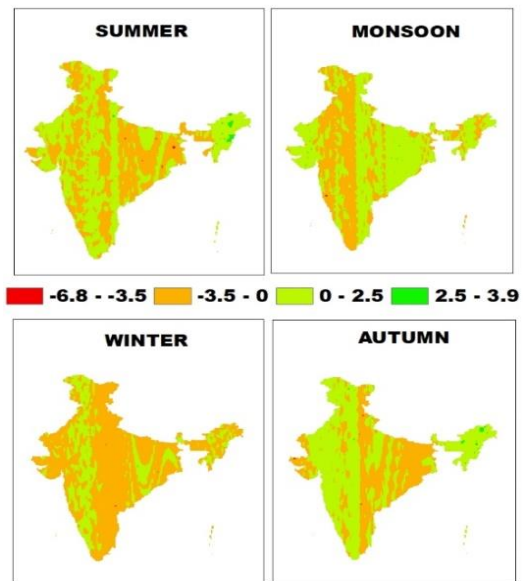


Fig. 4.4 SSP1 far future Z value

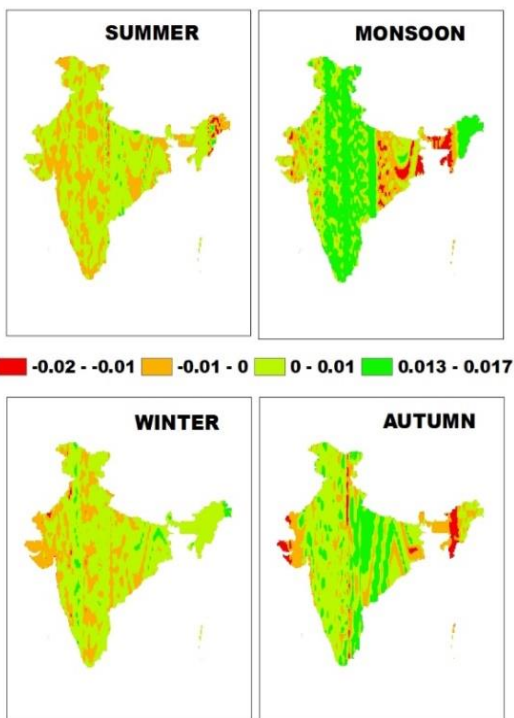


Fig. 4.5 SSP1 near future Sen's slope value

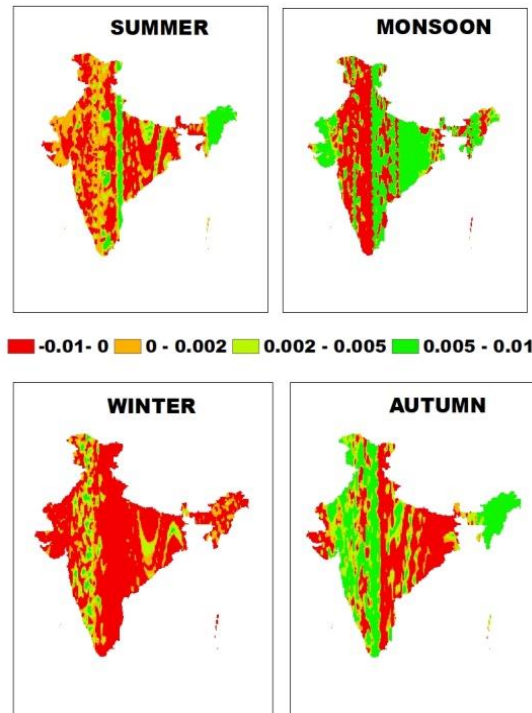


Fig. 4.6 SSP1 far future Sen's slope value

SSP1 near future Sen's slope value is shown in figure 4.5. In the near future, precipitation during summer and winter seasons is lesser but the north, central, southern and eastern parts of the country receive more precipitation during the monsoon and central parts along with some longitudinal strips from north to south receives more during the autumn.

SSP1 far future Sen's slope value is shown in figure 4.6. In the far future, precipitation shows a positive shift towards eastern region in monsoon and the autumn shift towards the western regions. During the winter season, precipitation all over the country is less and almost uniform.

4.2.1.3 Future data-SSP 2

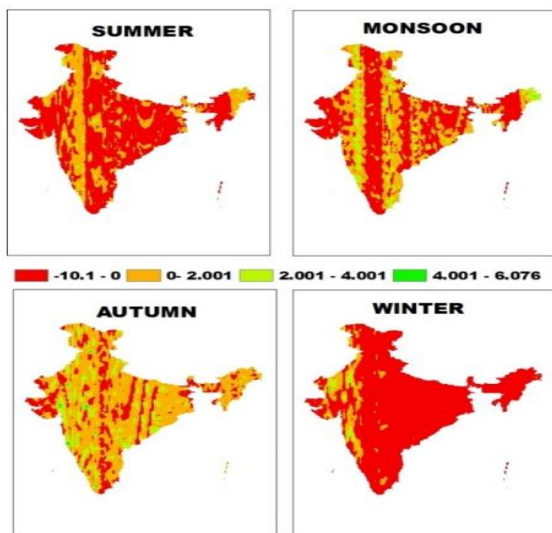


Fig. 4.7 SSP2 near future Z value

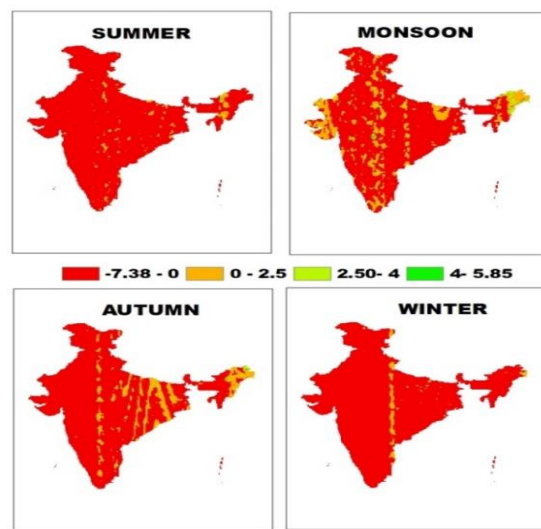


Fig. 4.8 SSP2 far future Z value

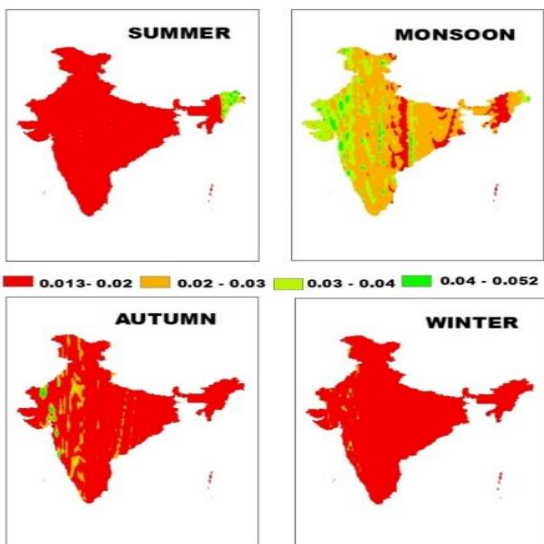


Fig. 4.9 SSP2 near future Sen's slope value

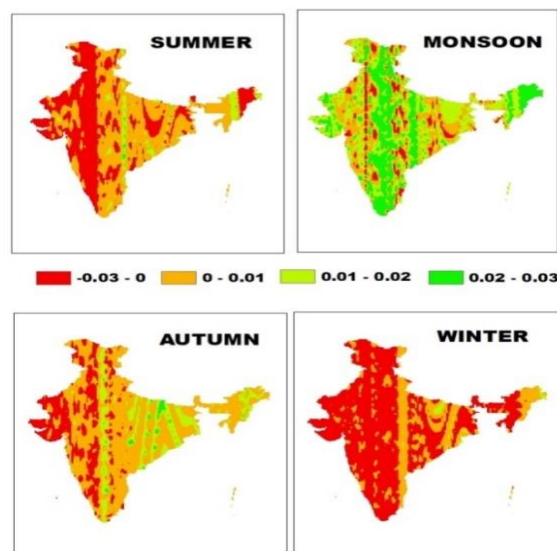


Fig. 4.10 SSP2 far future Sen's slope value

SSP2 near future Z value is shown in figure 4.7. SSP2 far future Z value is shown in figure 4.8. SSP2 near future Sen's slope value is shown in figure 4.9. SSP2 far future Sen's slope value is shown in figure 4.10. In this case, the range of Z and Sen's slope value is increased compared to previous SSP 1 case, also rainfall severely shows decreasing trend for most of the season and country except for the monsoons.

4.2.1.4 Future data-SSP 3

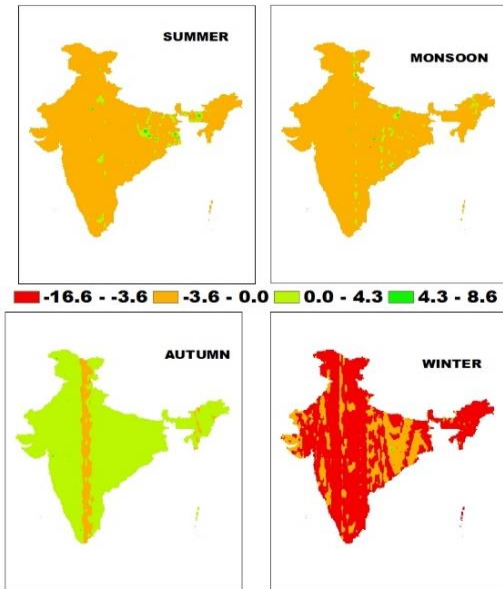


Fig. 4.11 SSP3 near future Z value

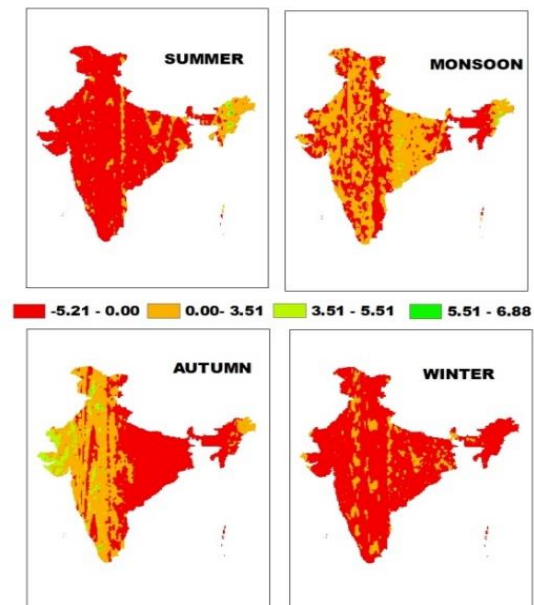


Fig. 4.12 SSP3 far future Z value

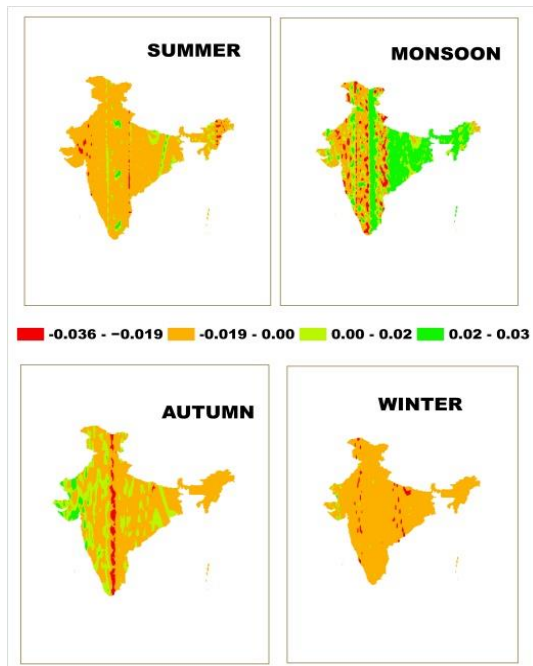


Fig. 4.13 SSP3 near future sen's slope value

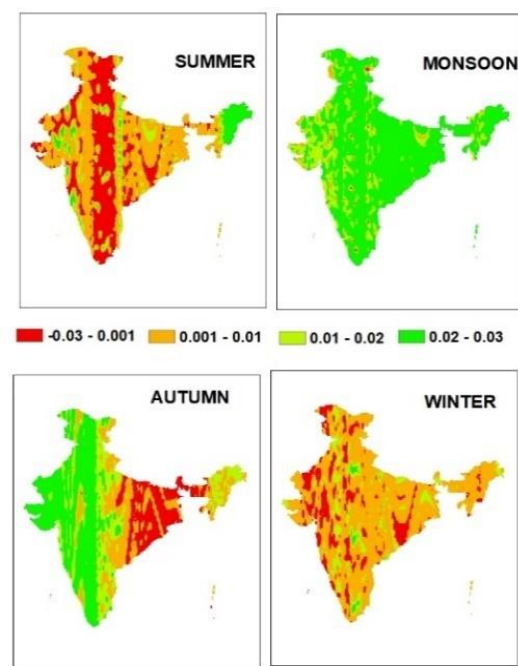


Fig. 4.14 SSP3 far future sen's slope value

SSP3 near future Z value is shown in figure 4.11. SSP3 near future sen's slope value is shown in figure 4.13. In the near future, during summer and winter, average precipitation is observed. During autumn season, western parts receive the maximum precipitation and other regions receive moderate precipitation. During the monsoon season, almost all parts receive more rainfall, specifically the eastern parts.

SSP3 far future Z value is shown in figure 4.12. SSP3 far future sen's slope value is shown in figure 4.14. In the far future, precipitation tends to increase in almost all regions with least observations in the western parts despite not much high value. Autumn and winters tend to receive increased precipitation as compared to the older observations. During monsoon, almost all parts of the country receive increased precipitation.

4.2.1.5 Future data-SSP 5

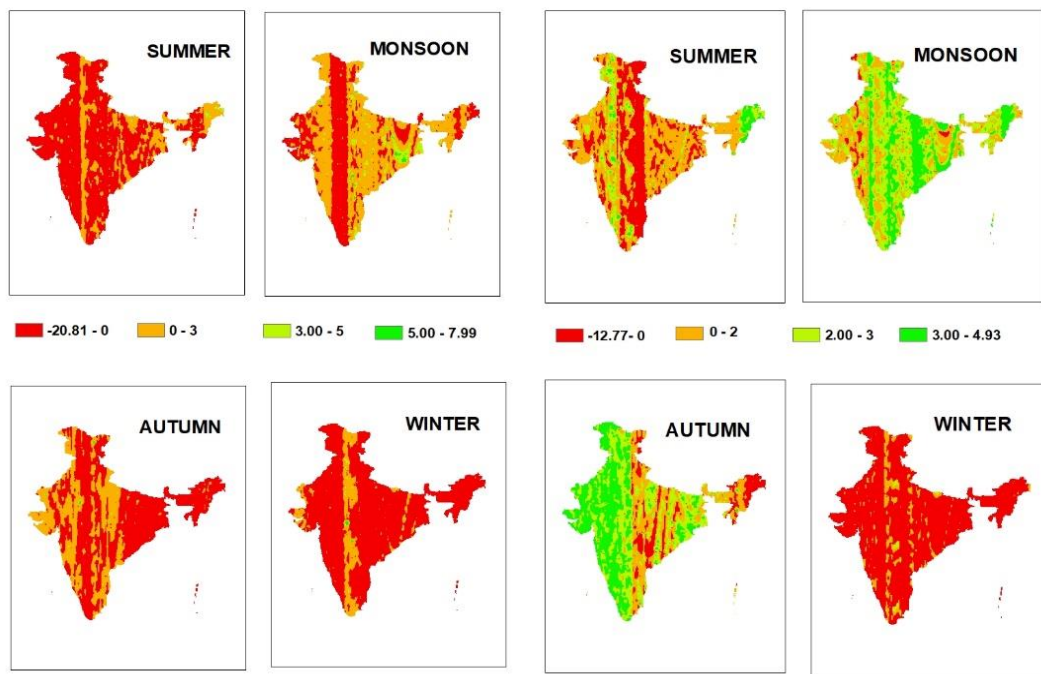


Fig. 4.15 SSP5 near future Z value

Fig. 4.16 SSP5 near future Z value

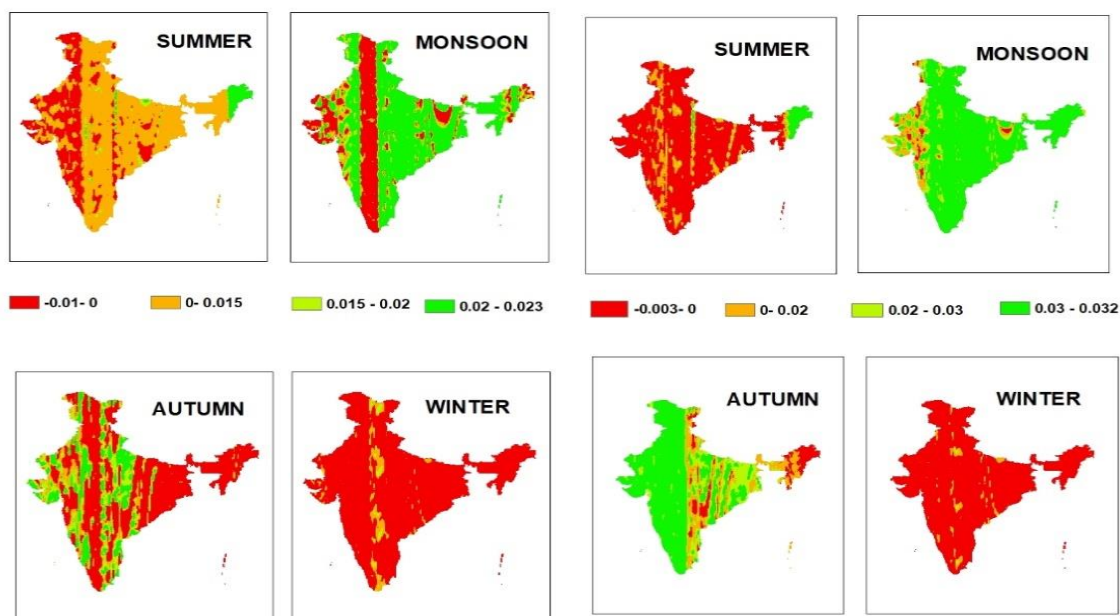


Fig. 4.17 SSP5 near future sen's slope value

Fig. 4.18 SSP5 far future Sen's slope value

SSP5 near future Z value is shown in figure 4.15 . SSP5 near future sen's slope value is shown in figure 4.17 . In the near future, during summer, precipitation seems to be very less in western parts while there is moderate precipitation in other parts of country. Winters seem to receive less precipitation whereas during autumn, precipitation is very less in the eastern regions and patches of areas with increase in precipitation are scattered in other parts of the country. The precipitation during monsoon is maximum for almost all the parts whereas it is very less for regions that lie on the longitudinal midline of the country from north to south.

SSP5 far future Z value is shown in figure 4.16. SSP5 far future Sen's slope value is shown in figure 4.18. In the far future, northeastern region receives more precipitation during summer and winter seems to have less precipitation all throughout the country. Increased precipitation is there in almost all parts except the eastern end during the autumn season whereas the monsoon season shows the increase in precipitation all throughout the country in the high emission scenario.

4.2.2 Maximum Temperature (T_{max})

The results of Modified Mann Kendall (Z values) and the Sen's slope tests done on the historical and the future datas of the considered 4 SSP scenarios are compared in order to understand the trend.

4.2.2.1 Historic data

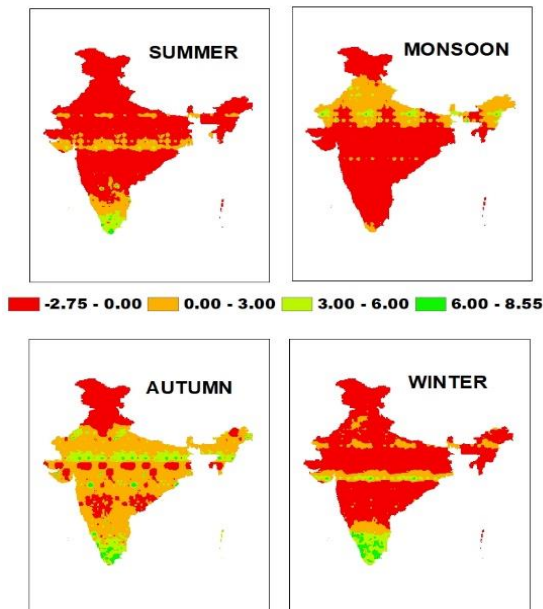


Fig. 4.19 Z value for trend analysis using historic data

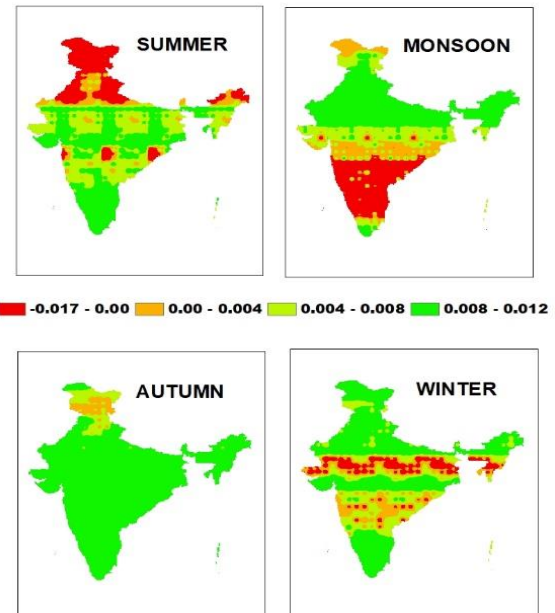


Fig. 4.20 Sen's slope value for trend analysis using historic data

Z value for trend analysis using historic data is shown in figure 4.19. Sen's slope value for trend analysis using historic data is shown in figure 4.20. During summer, all parts except Northern regions have higher temperatures. The trend shifts to all parts except south east and south west during the monsoon. All over the country, temperature received is more in autumn and in winters, transverse central parts receive lesser temperature.

4.2.2.2 Future data-SSP 1

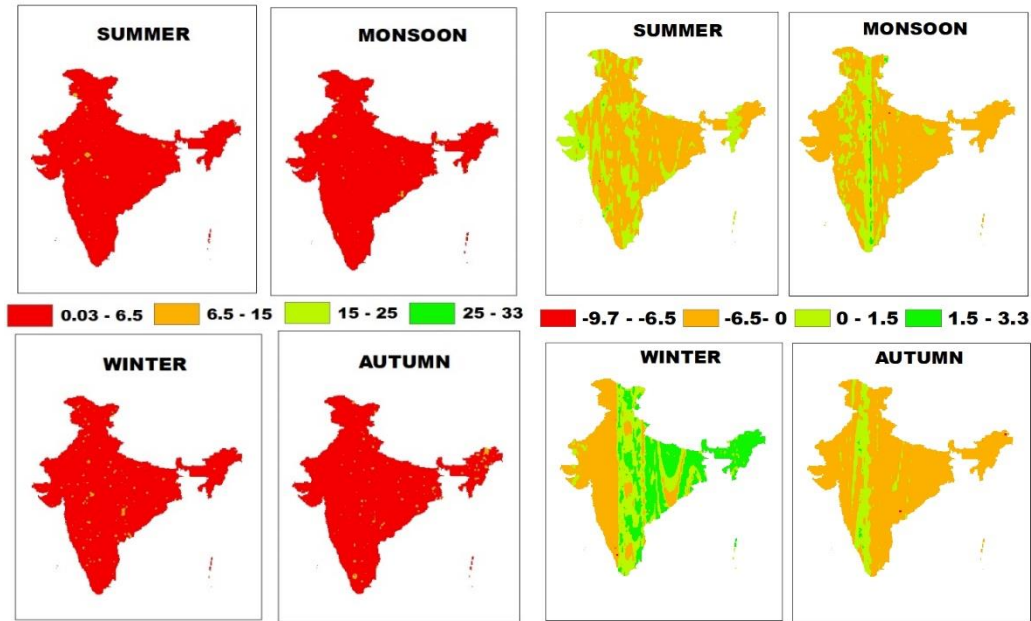


Fig. 4.21 SSP1 near future Z value Fig. 4.22 SSP1 far future Z value

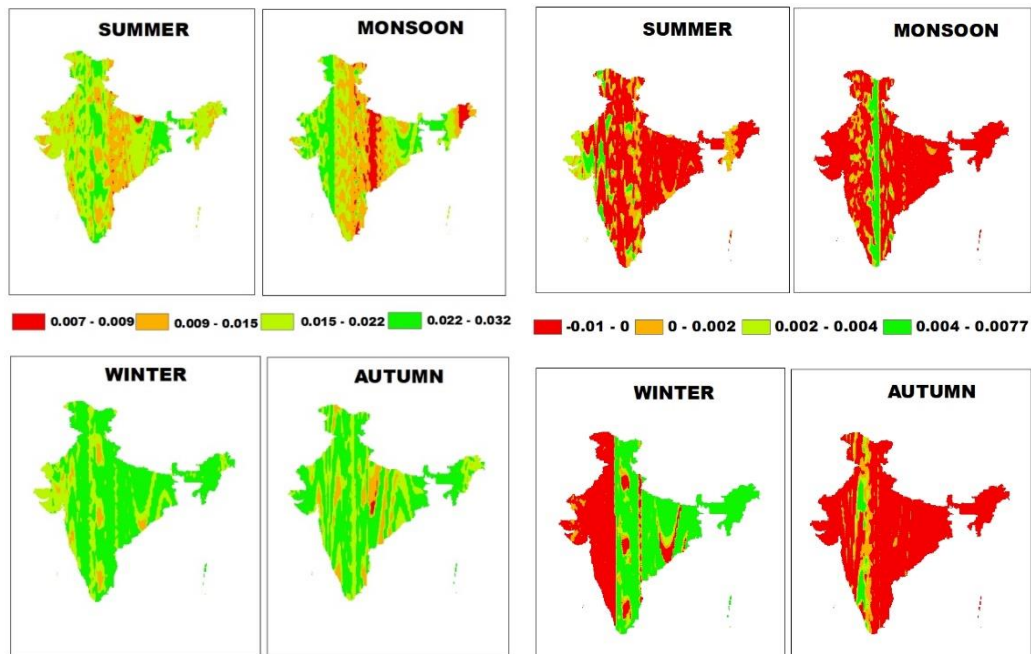


Fig. 4.23 SSP1 near future sen's slope value

Fig. 4.24 SSP1 far future Sen's slope value

SSP1 near future Z value is shown in figure 4.21. SSP1 near future sen's slope value is shown in figure 4.23. SSP1 far future Z value is shown in figure 4.22. SSP1 far future Sen's slope value 4.24. In the near future, maximum temperature in all regions tends to

increase except in some central areas during monsoon. In far future, it tends to decrease in all seasons except in the eastern part of the country with an increase during the winter season.

In the sustainable path based SSP 1 scenario, overall the Tmax value is under control without much increase. Besides, the maximum value of range is also too less.

4.2.2.3 Future data SSP-2

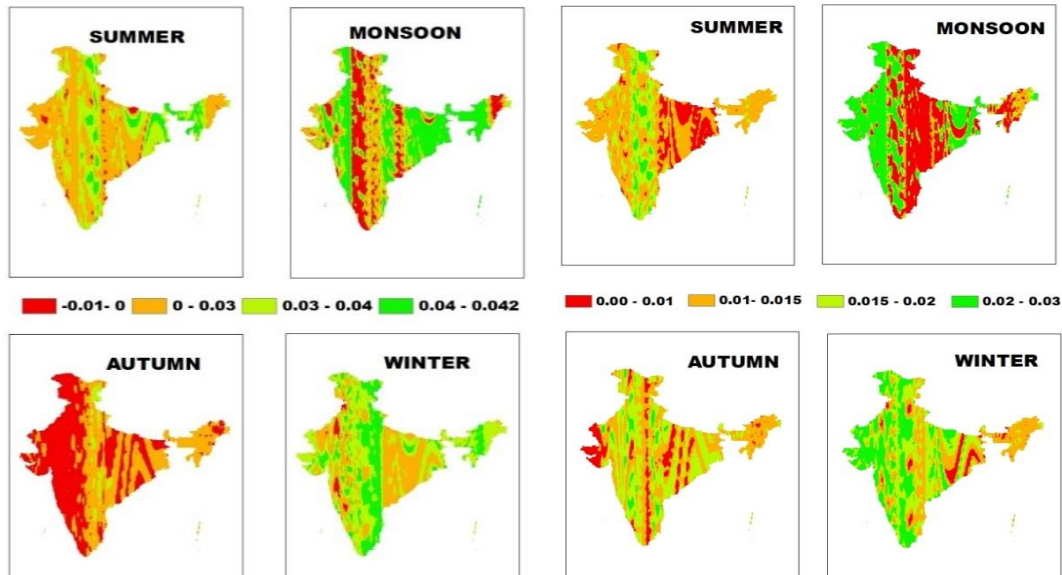


Fig. 4.25 SSP2 near future Z value

Fig. 4.26 SSP2 far future Z value

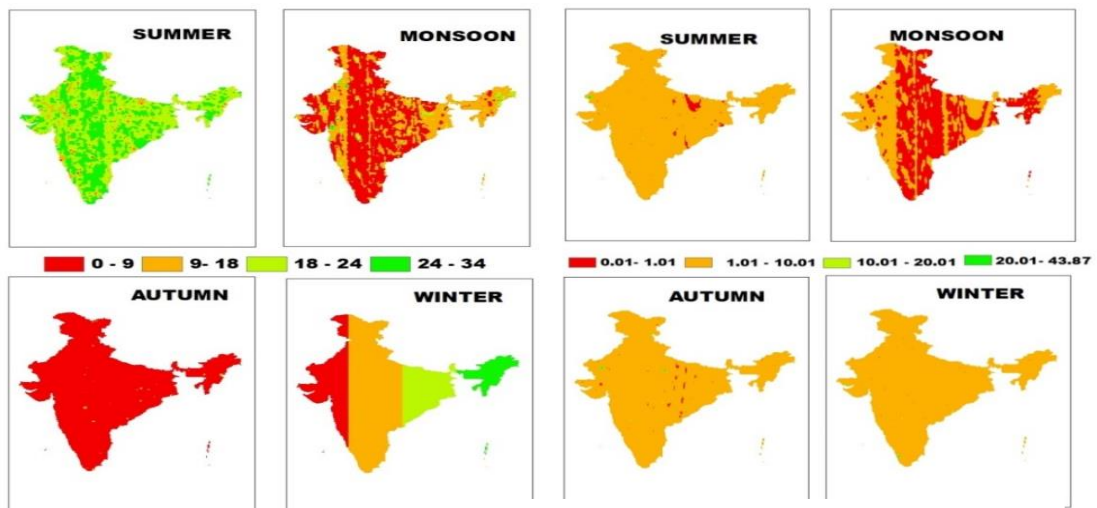


Fig. 4.27 SSP2 near future sen's slope value

Fig. 4.28 SSP2 far future Sen's slope value

SSP2 near future Z value is shown in figure 4.25. SSP2 near future sen's slope value is shown in figure 4.27. In the near future, Tmax shows an increasing trend in summer, monsoon and winter in almost all parts of country except a decrease is observed for the longitudinal midland in monsoon. In autumn, Tmax has a decreasing trend.

SSP2 far future Z value is shown in figure 4.26. SSP2 far future Sen's slope value is shown in figure 4.28. In the far future, almost all parts of the country receive increased Tmax. But in monsoon, slightly eastward longitudinal midland shows a decrease in the maximum temperature.

4.2.2.4 Future data- SSP 3

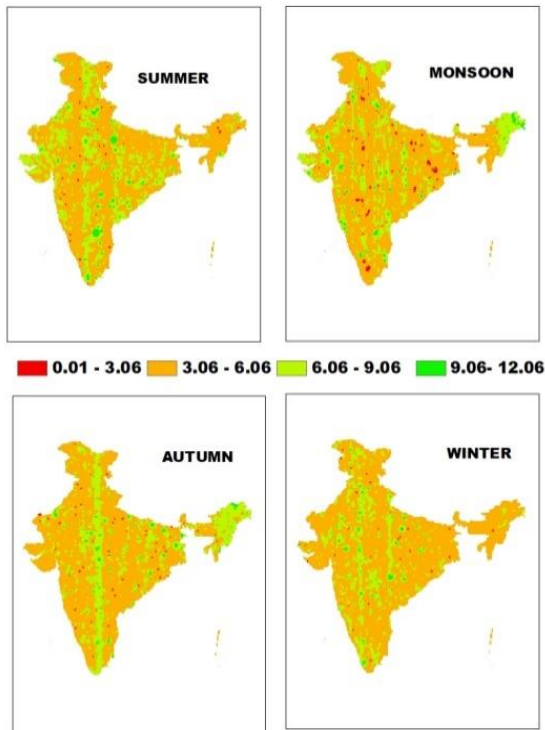


Fig. 4.29 SSP3 near future Z value

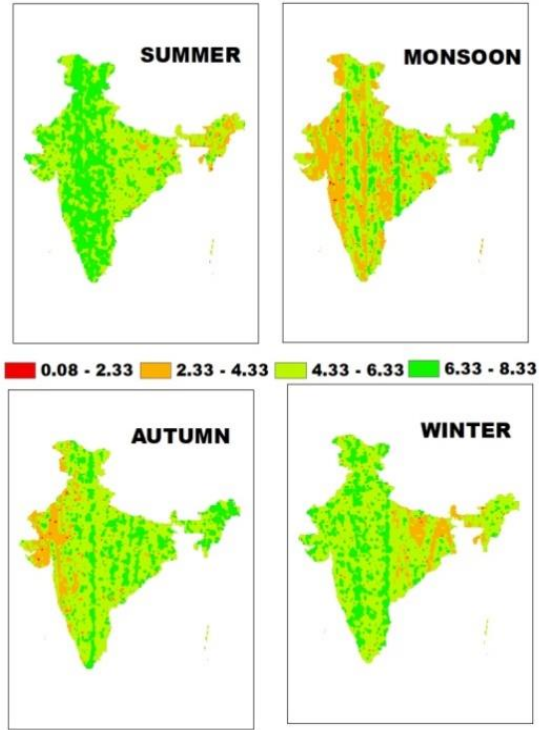


Fig. 4.30 SSP3 far future Z value

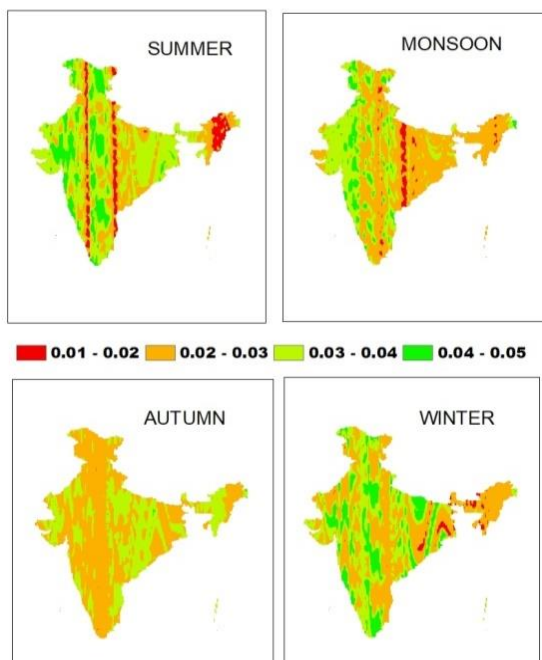


Fig. 4.31 SSP3 near future Sen's slope value

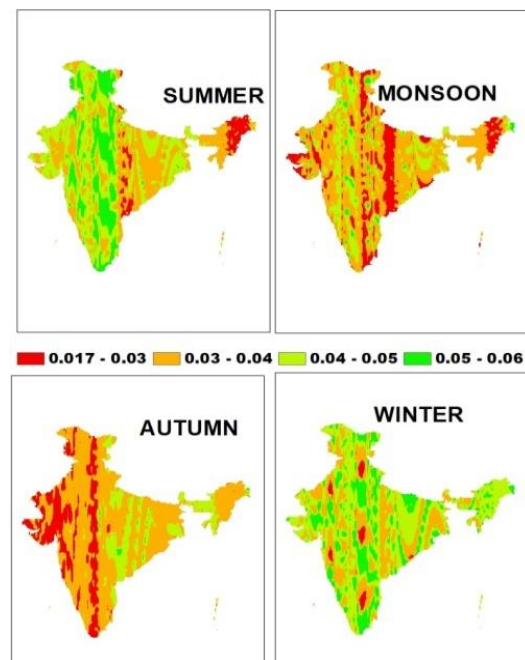


Fig. 4.32 SSP3 far future Sen's slope value

SSP3 near future Z value is shown in figure 4.29. SSP3 near future sen's slope value is shown in figure 4.31. In the near future, maximum temperature all across the country in all the 4 seasons show a drastic increase with exception of small areas of North-East receiving lesser Tmax in summer.

SSP3 far future Z value is shown in figure 4.30. SSP3 far future Sen's slope value is shown in figure 4.32. In the far future, trend is similar as of near future, but with a relatively small increasing value. The Tmax shows a decreasing trend in certain parts during monsoon and autumn.

4.2.2.5 Future data- SSP 5

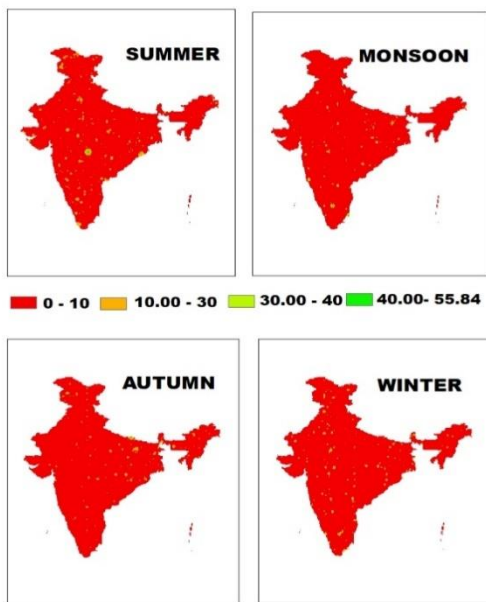


Fig. 4.33 SSP5 near future Z value

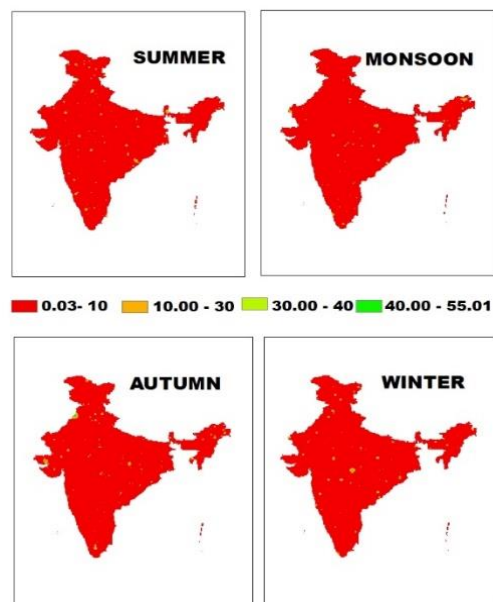


Fig. 4.34 SSP5 far future Z value

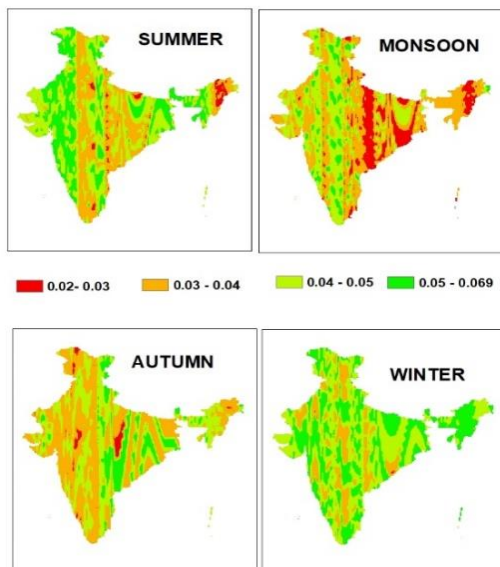


Fig. 4.35 SSP5 near future Sen's slope value

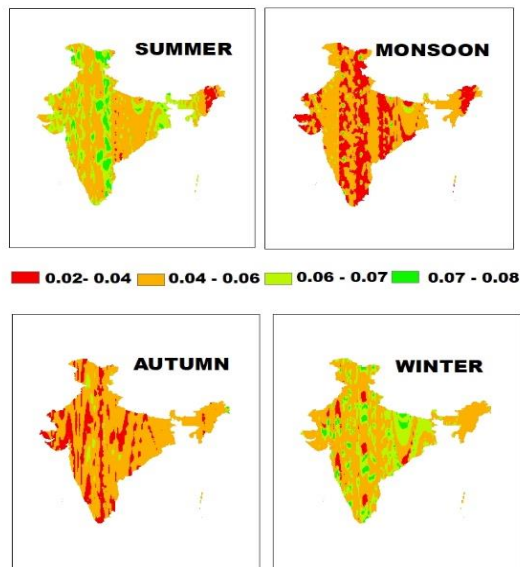


Fig. 4.36 SSP5 far future Sen's slope value

In the risky high emission scenario, most of the country shows remarkable increasing trend as per the Z-value compared to previous SSP scenarios.

SSP5 near future Z value is shown in figure 4.33. SSP5 near future sen’s slope value is shown in figure 4.35. In the near future, all parts of the country experience high temperatures with the exception of some places in eastern strip receiving lesser temperature in the monsoon.

SSP5 far future Z value is shown in figure 4.34. SSP5 far future sen’s slope value is shown in figure 4.36. In the far future, Tmax all over the country during all seasons is high, but not as much as in the near future.

4.2.3 Minimum Temperature (T_{min})

The results of Modified Mann Kendall (Z values) and the Sen’s slope tests done on the historical and the future data’s of the considered 4 SSP scenarios are compared in order to understand the trend.

4.2.3.1 Historical data

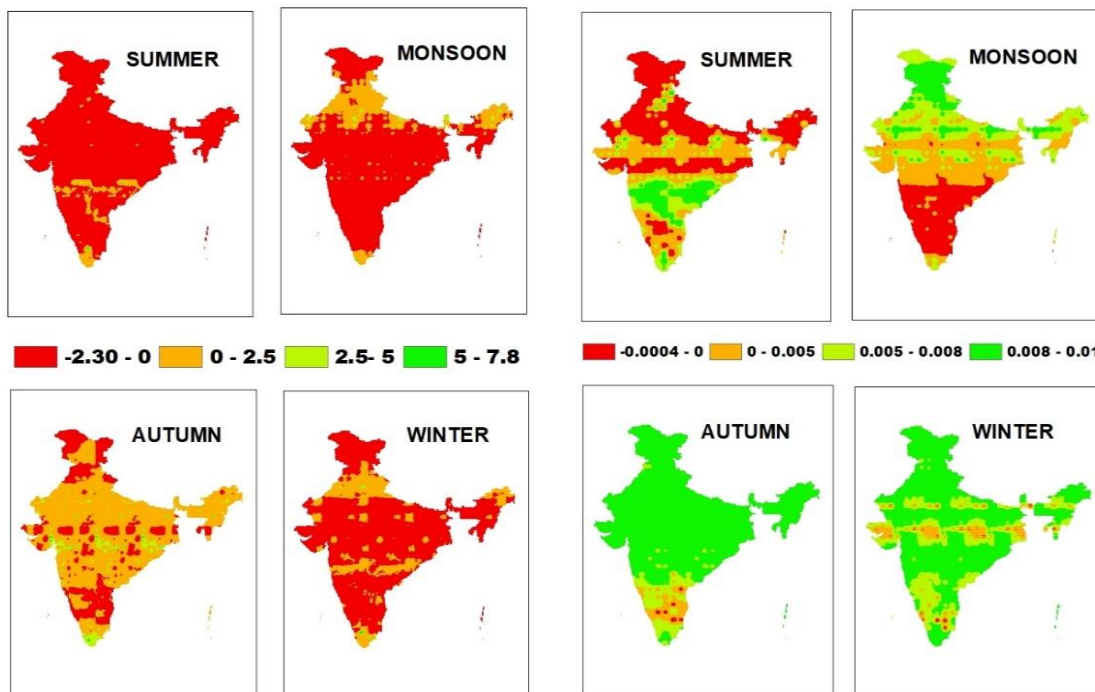


Fig. 4.37 Z value for trend analysis using historic data

Fig. 4.38 Sen’s slope value for trend analysis using historic data

Z value for trend analysis using historic data is shown in figure 4.37. Sen’s slope value for trend analysis using historic data is shown in figure 4.38.

4.2.3.2 Future data- SSP 1

Tmin shows a decreasing trend for most of the country for almost seasons. The increasing trend is not remarkable as it was for observed historic data. The minimum temperature is more during the autumn and winter seasons in almost all throughout the country with some exceptions.

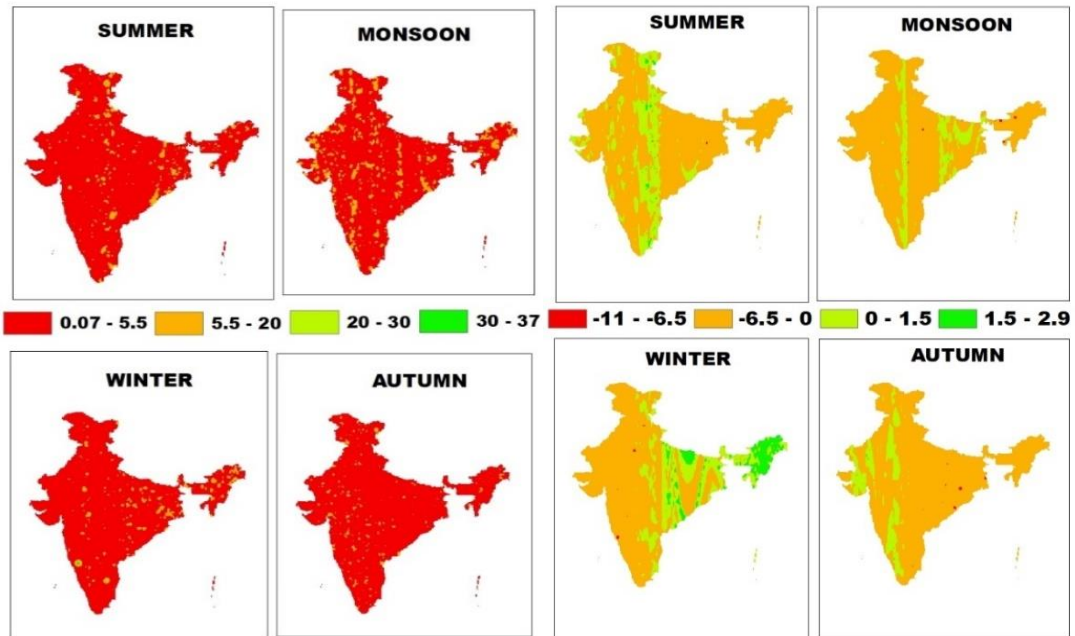


Fig. 4.39 SSP1 near future Z value

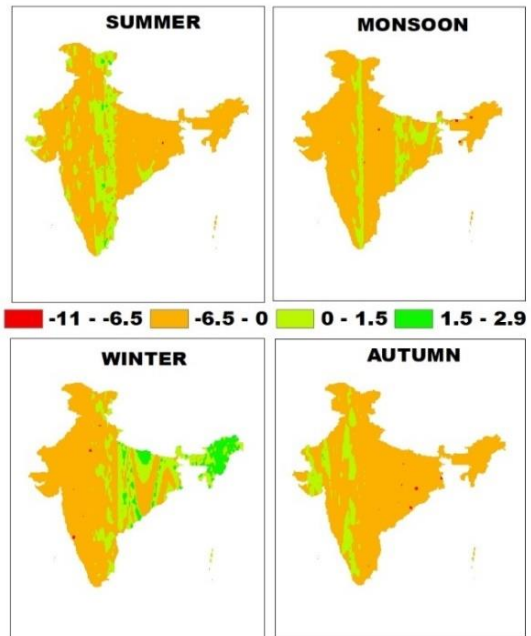


Fig. 4.40 SSP1 far future Z value

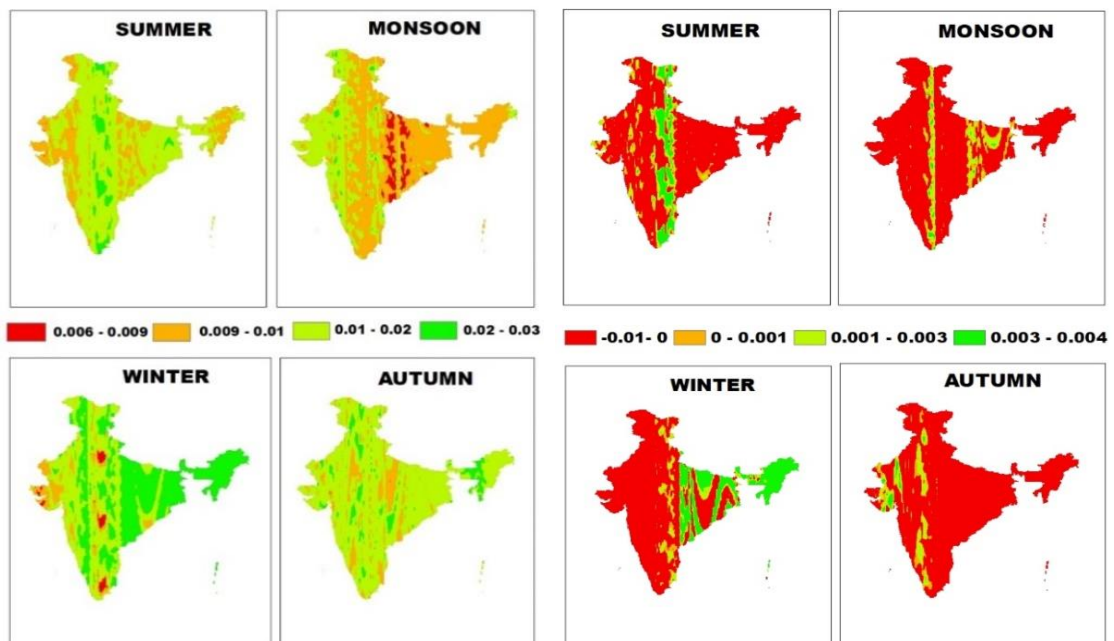


Fig. 4.41 SSP1 near future Sen's slope value

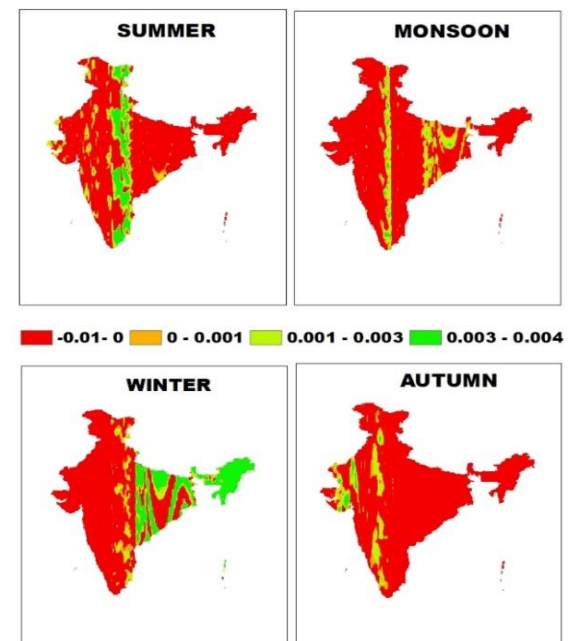


Fig. 4.42 SSP1 far future Sen's slope value

SSP1 near future Z value is shown in figure 4.39. SSP1 near future sen's slope value is shown in figure 4.41. In the near future, Tmin is increased in almost all parts of the country with a slight decrease in the trend during the monsoon in eastern parts.

SSP1 far future Z value is shown in figure 4.40. SSP1 far future sen's slope value is shown in figure 4.42. In the far future, Tmin has a decreasing trend in almost all the parts during all the 4 seasons. With an overall positive trend almost all over, it shows an increase only in certain parts of north east in winter.

4.2.3.3 Future data- SSP 2

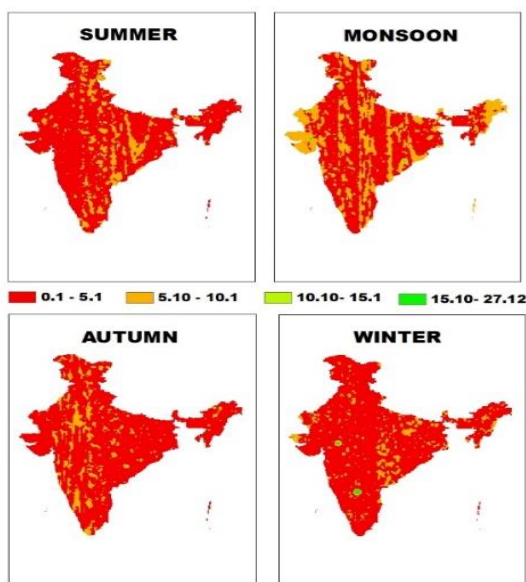


Fig. 4.43 SSP2 near future Z value

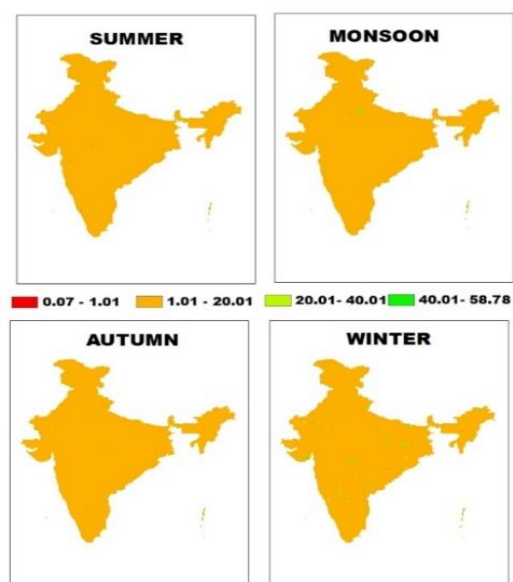


Fig. 4. 44 SSP2 far future Z value

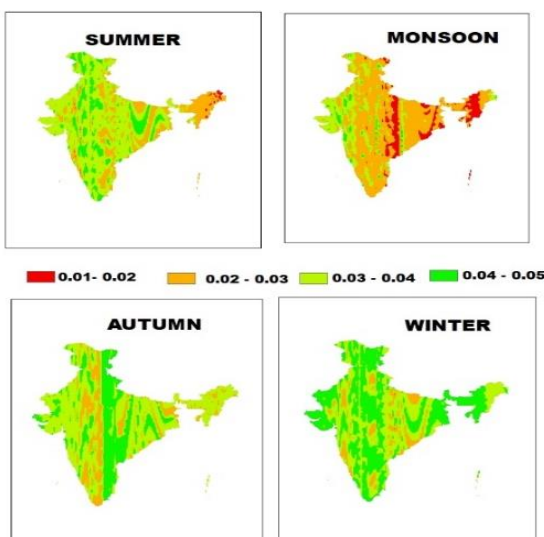


Fig. 4.45 SSP2 near future sen's slope value

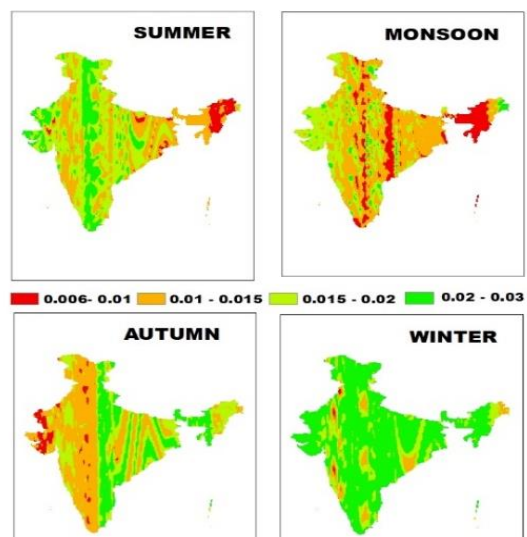


Fig. 4.46 SSP2 near future sen's slope value

SSP2 near future Z value is shown in figure 4.43. SSP2 near future sen's slope value is shown in figure 4.45. In the near future, Tmin is increased all over the country in four seasons. During monsoon, all the parts except the western end regions experience the decrease in minimum temperature.

SSP2 far future Z value is shown in figure 4.44. SSP2 far future sen's slope value is shown in figure 4.46. In the far future, the same trend as of the near future is observed. During the monsoon, Tmin has a decreasing trend in the eastern regions and during the autumn, eastern regions tend to have decrease in the minimum temperature.

4.2.3.4 Future data- SSP 3

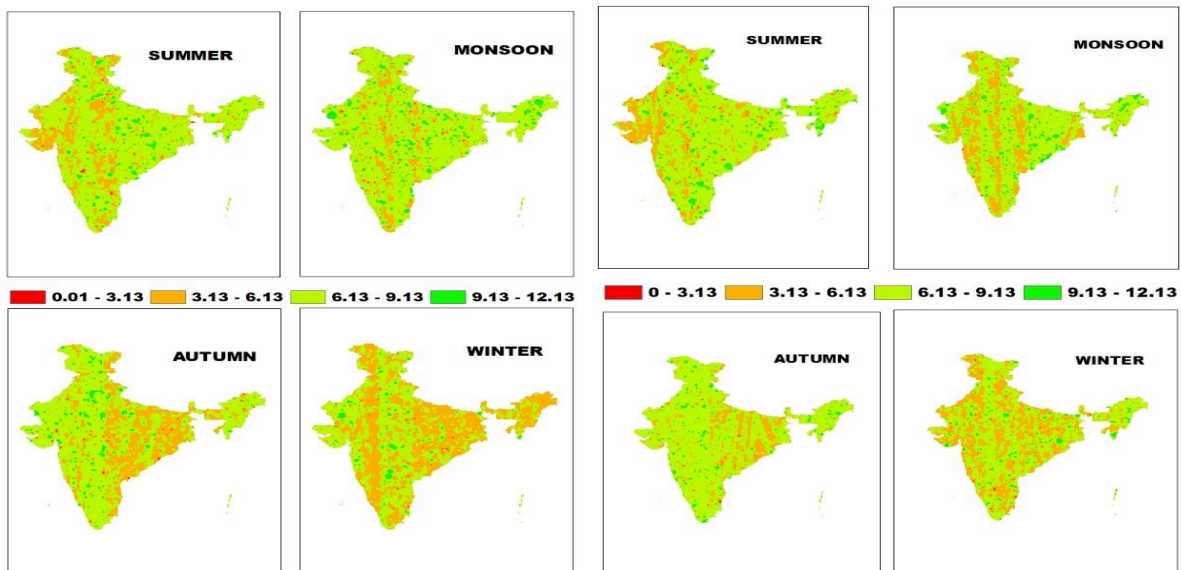


Fig. 4.47 SSP2 near future Z value

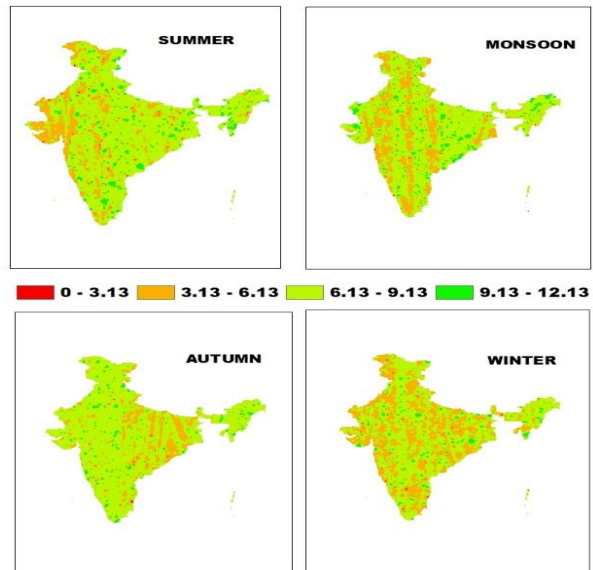


Fig. 4.48 SSP2 near future Z value

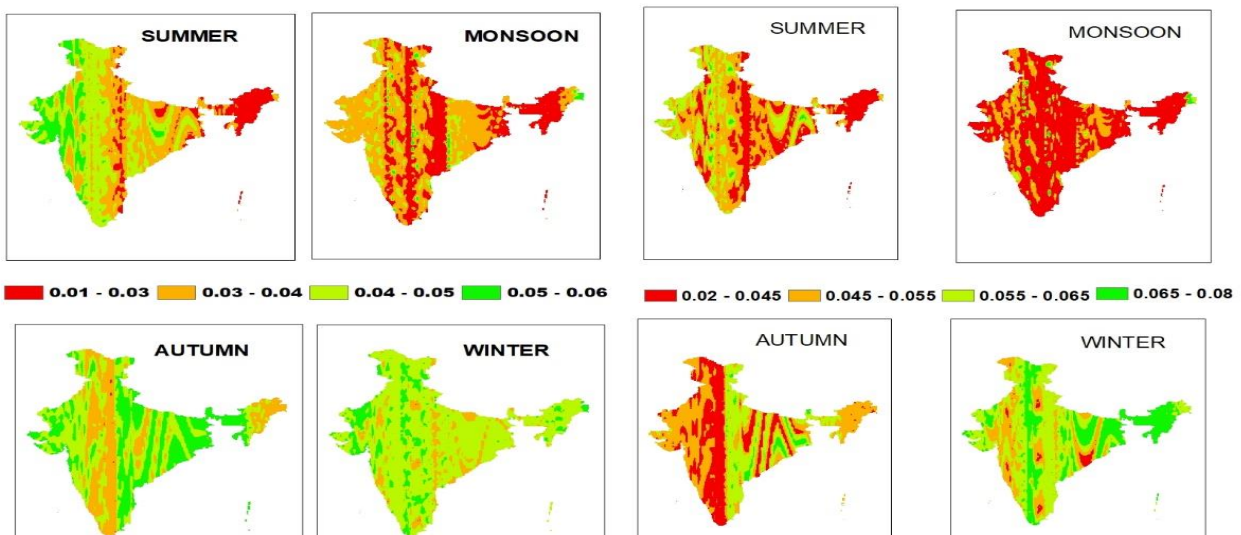


Fig. 4.49 SSP3 near future sen's slope value

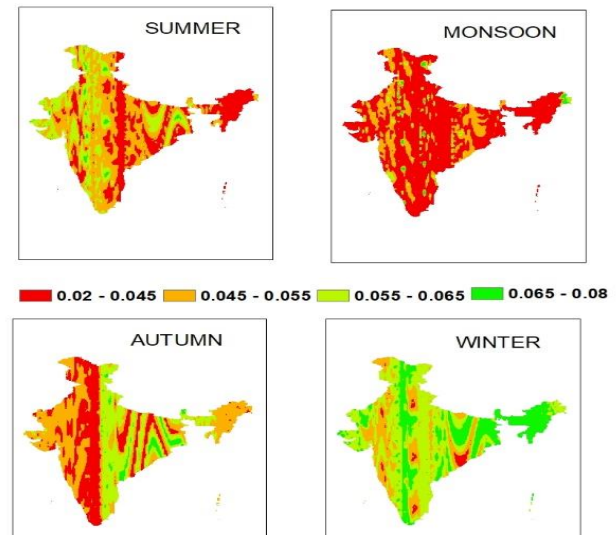


Fig. 4.50 SSP3 far future Sen's slope value

SSP3 near future Z value is shown in figure 4.47. SSP3 near future sen's slope value is shown in figure 4.49. SSP3 far future Z value is shown in figure 4.48. SSP3 far future sen's slope value is shown in figure 4.50. In the near future, for all seasons except monsoon, the Tmin is increasing. In the far future, during summer, monsoon and autumn, Tmin is decreasing, but in autumn, the eastern parts receive increased Tmin. During the winter season, Tmin all across the country is increased.

4.2.3.5 Future data- SSP 5

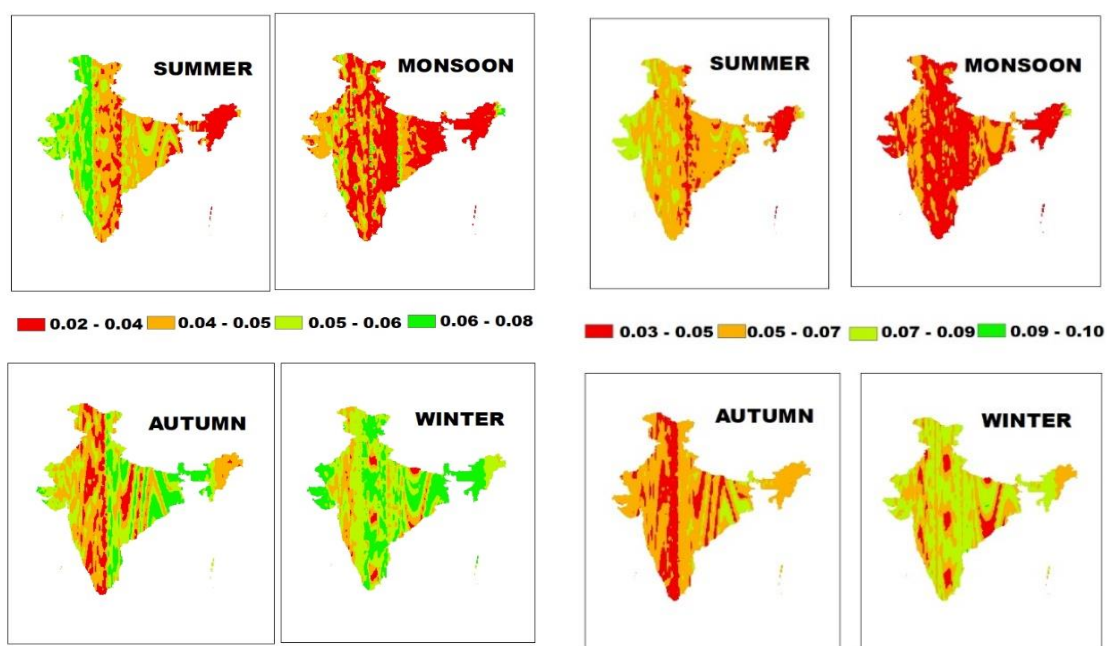


Fig. 4.51 SSP5 near future Z value

Fig. 4.52 SSP5 far future Z value

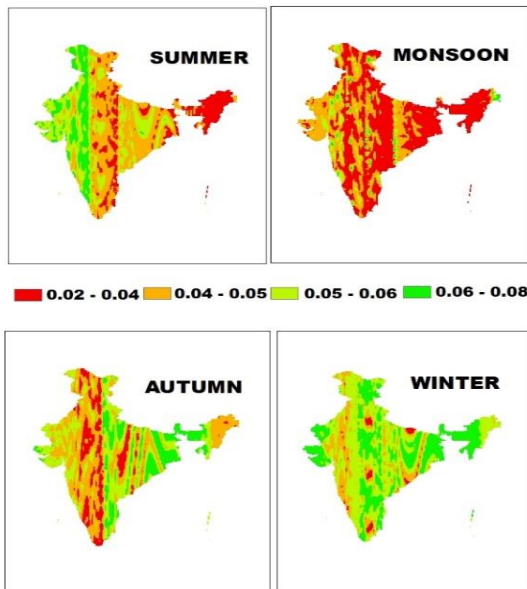


Fig. 4.53 SSP5 near future sen's slope value

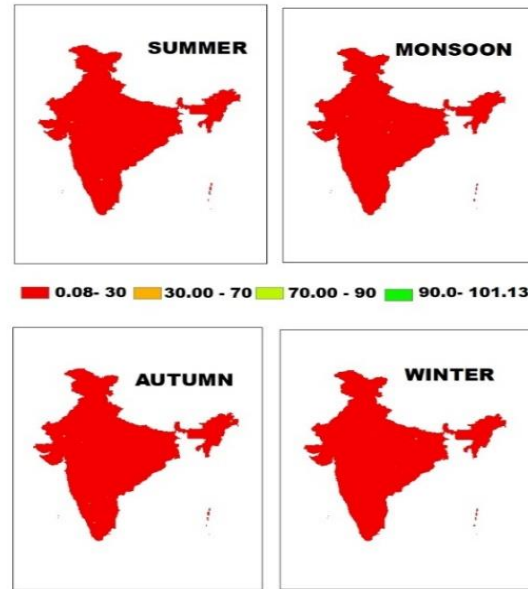


Fig. 4.54 SSP5 far future Sen's slope value

SSP5 near future Z value is shown in figure 4.51. SSP5 near future sen's slope value is shown in figure 4.53. In the near future, Tmin during the summer season is decreased in the country but in the eastern regions, the Tmin is more. The Tmin is decreased in all parts during monsoon and in autumn and winter, there is an increasing trend in the Tmin.

SSP5 far future Z value is shown in figure 4.52. SSP5 far future sen's slope value is shown in figure 4.54. In the far future, Tmin all across the country is decreased in all the 4 seasons but during winter, there is an increase in the Tmin all throughout the country.

The simulated future rainfall and temperature variable all are showing positive trend up to the end of the 21st century except few variation in some cases. In the past historic trend, except southern region, remaining region showed decreasing trend particularly for the Monsoon season, but the future monsoon showed pan India increasing pattern for all the four SSP cases. Similarly, the future surface air temperature is also observed to have a positive trend for all the four seasons through the India. The increasing temperature has chances to influence precipitation extremes.

The Coefficient of Variation (C.V.) is a statistical measure of the relative variability of a dataset. It is calculated as the ratio of the standard deviation to the mean, often expressed as a percentage. A higher C.V. indicates greater variability relative to the mean.

Table 4.4 Coefficient of Variation (C.V.) of the future

	SSP126	SSP245	SSP370	SSP586
SUMMER	46	50	47	48
MONSOON	24	23	27	27
AUTUMN	37	15	40	39
WINTER	46	54	51	49

Here the C.V. of future precipitation for four different scenarios (SSP126, SSP245, SSP370, SSP586) across four seasons (summer, monsoon, autumn, winter) is depicted.

The C.V. values for summer precipitation are relatively high across all scenarios, with SSP245 showing the highest variability (50%) and SSP126 the lowest (46%). This suggests that, regardless of the scenario, summer precipitation is expected to have considerable variability.

Monsoon precipitation shows lower variability compared to other seasons, with C.V. values ranging from 23% to 27%. SSP245 exhibits the least variability (23%), while SSP370 and SSP586 are tied for the highest variability (27%). Variability increases slightly in the higher emission scenarios, which indicates there is a chance of sudden precipitations that may lead to flash floods.

Autumn precipitation variability shows significant differences between scenarios. SSP245 has the lowest C.V. (15%), indicating more stable precipitation. In contrast, SSP370 has the highest variability (40%), suggesting more fluctuation in precipitation levels.

Winter precipitation variability is high across all scenarios, with SSP245 showing the highest C.V. (54%) and SSP126 the lowest (46%). This indicates that winter precipitation is expected to be quite variable, especially in SSP245.

Overall, these patterns can help inform water resource management, agricultural planning, and disaster preparedness by highlighting the expected variability in precipitation under different future scenarios.

4.3 IDENTIFICATION OF CHANGE POINT IN UPCOMING TIME PERIOD FOR THE METEOROLOGICAL VARIABLES

The Pettit change point test was used to identify a single change point in a time series. It is essential in the analysis of climate and hydrological data to detect a shift or an abrupt change.

4.3.1 SSP1

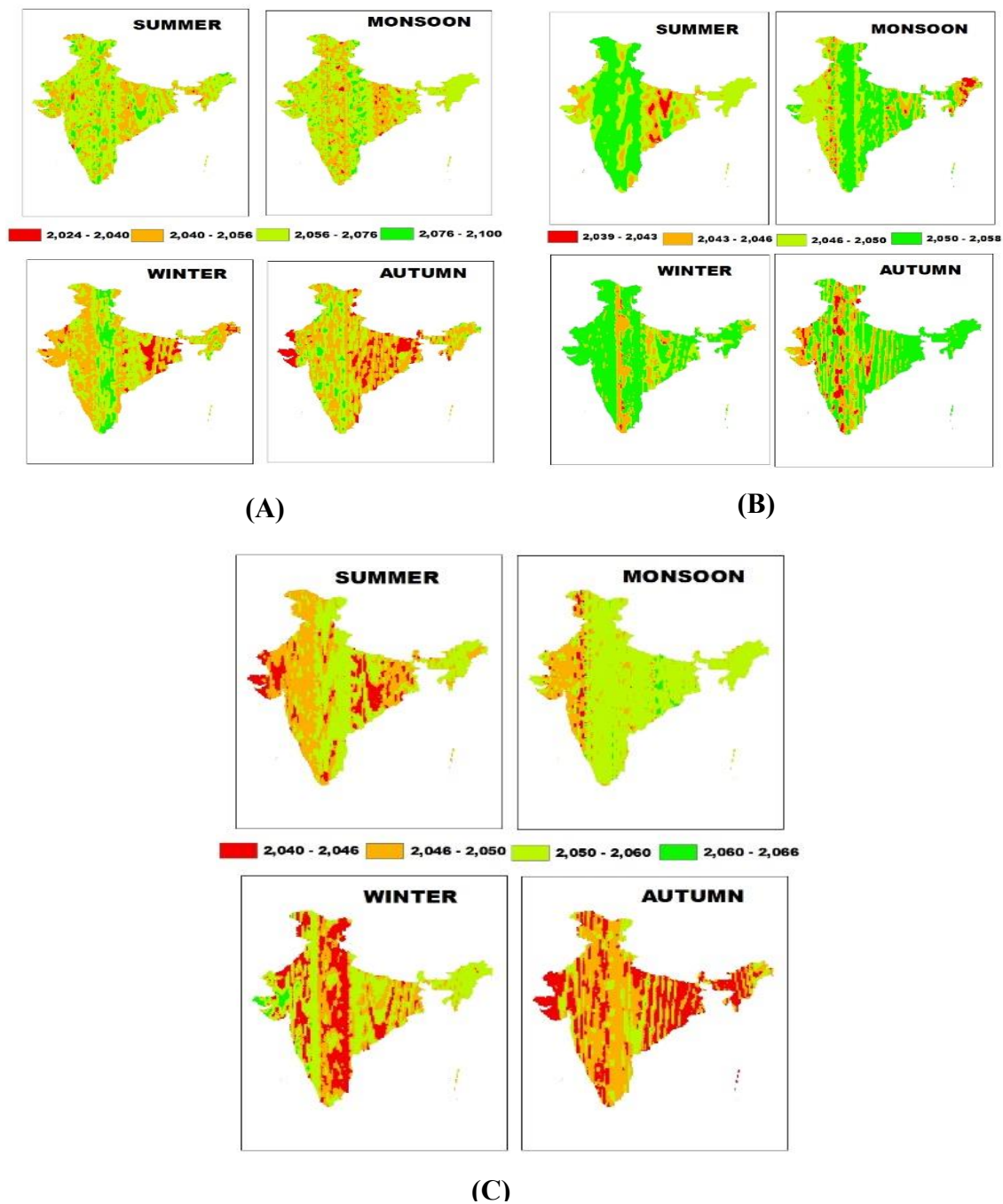


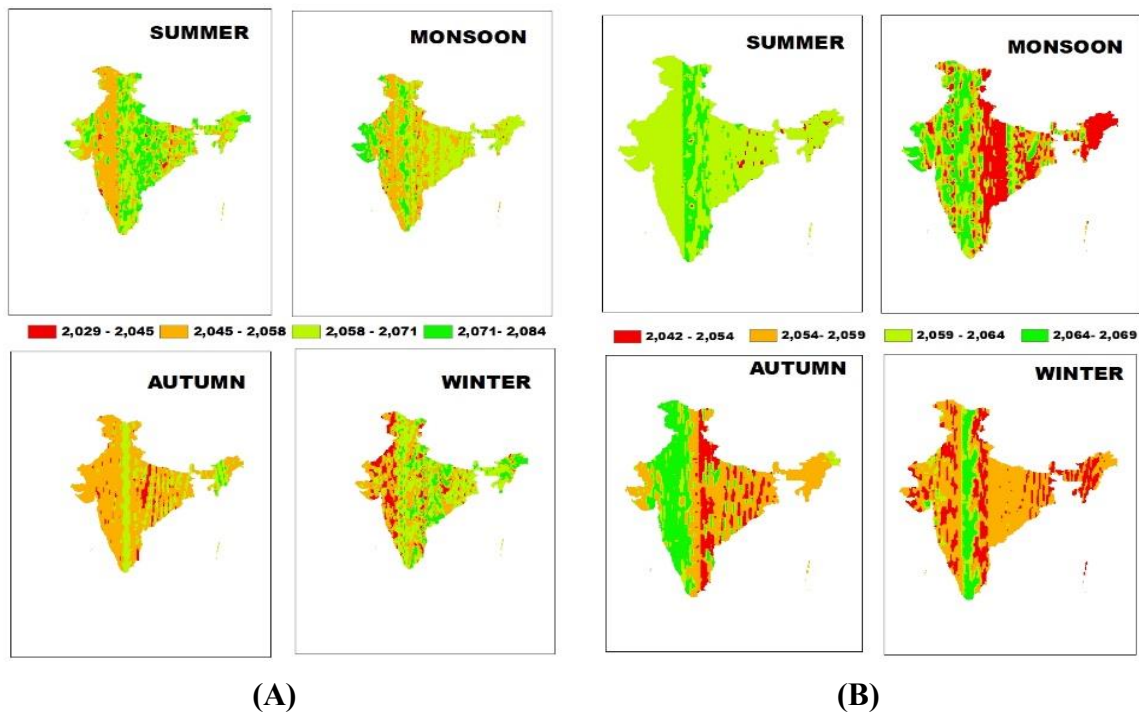
Fig. 4.55 Change point analysis of future data for SSP1 (A) Precipitation (B) T max (C) Tmin

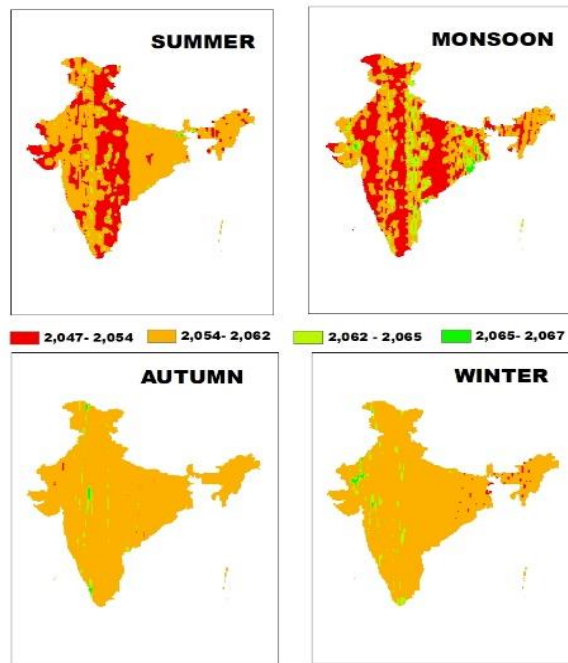
For precipitation, changes in almost all the parts of the country are expected to happen between 2056 and 2100 during summer and monsoon. During winter, the longitudinal midland shows the change during 2076-2100. Some north-eastern areas seems to experience the change in precipitation earlier from 2024-2040 period during autumn and winter with the addition of the western end experiencing similar earlier precipitation change during autumn.

For Tmax, all the seasons experience the change during 2050-2055 period in almost all areas except some. In summer, the change of Tmax in the north eastern parts happen early during 2039-2043 whereas in autumn this early change occurs in certain strips in the western parts.

For Tmin, during summer, the western end and north eastern parts experience early change during 2040-2046 and in monsoon, almost all changes occur during 2046 -2060. Winter and autumn season experience earlier changes in Tmax during 2040-2060 time frame.

4.3.2 SSP2





(C)

Fig. 4.56 Change point analysis of future data for SSP2 (A) Precipitation (B) T max (C) Tmin

For precipitation, almost all the parts experience the change during 2045-2084 in the summer and monsoon whereas in autumn, most changes occur during 2045-2071 timeframe. In the winter, almost all areas experience changes from 2045 to 2084 but the western ends experience early changes during 2029-2045.

For Tmax, changes in summer all over India occurs during 2059- 2069. In monsoon and autumn, early changes happen towards the eastern parts of the country during the 2042- 2059 timeframe. In winter, almost all areas experience early changes (2042- 2059) with the exception of central longitudinal midland experiencing the change during 2064-2069.

For Tmin, for all the seasons, early changes are observed between the 2047- 2062 timeframe.

4.3.3 SSP3

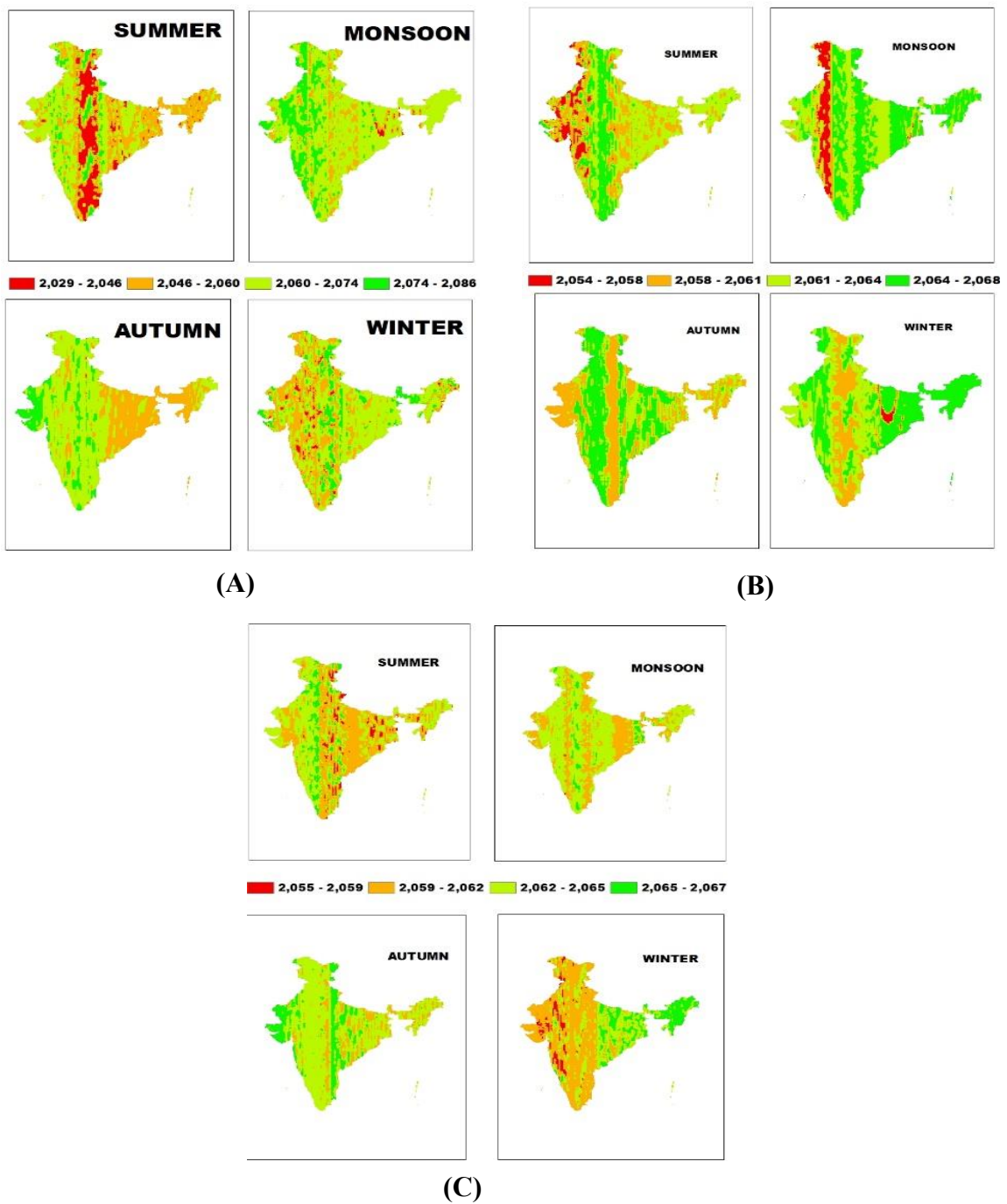


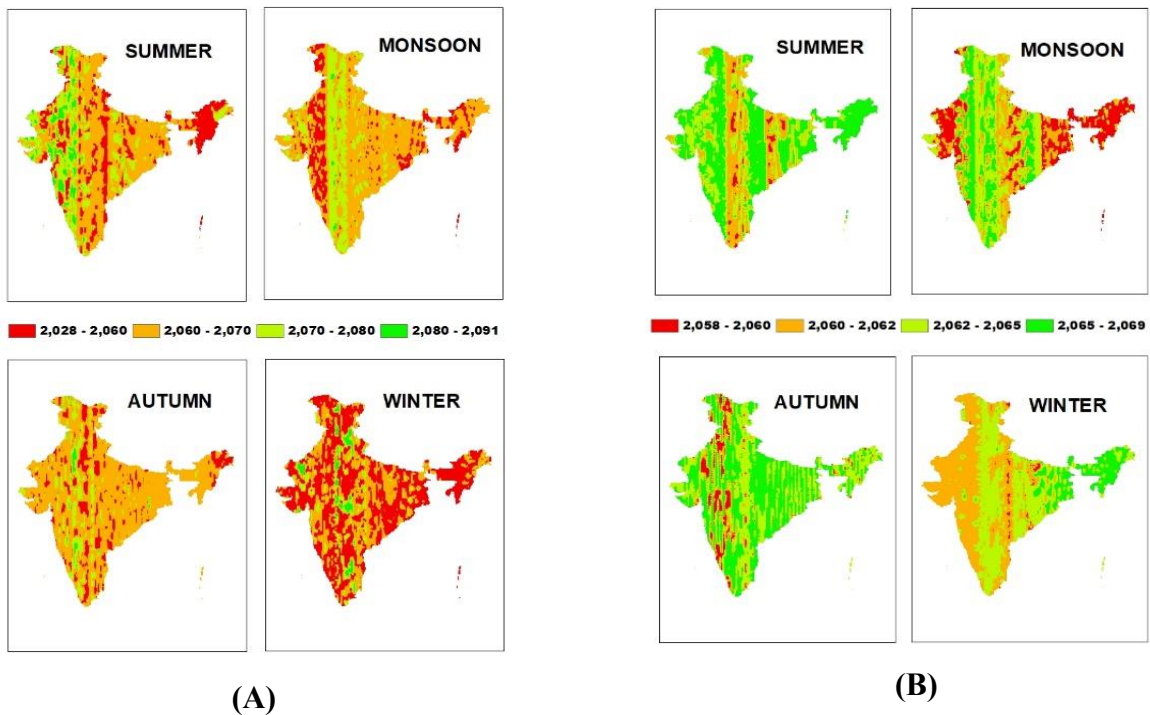
Fig. 4.57 Change point analysis of future data for SSP3 (A) Precipitation (B) T max (C) Tmin

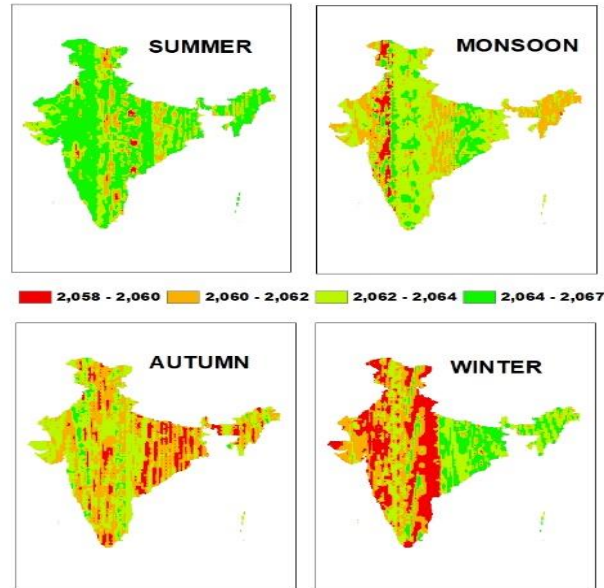
For Precipitation, all the changes occur during the 2046-2086 timeframe in almost all parts of the country with the exception of early changes during the 2029- 2046 time period in the summer seasons across the longitudinal midland.

For Tmax, changes in all the seasons occur mainly during 2058-2068 whereas during summer and monsoon, certain areas in the western side experience early change during the 2054- 2058 timeframe.

For Tmin, all changes occur between 2059 and 2067. Certain strips across the midland and north east experience changes during 2055- 2059 in summer and some areas of western India experience the change in the early 2055-2059 timeframe.

4.3.4 SSP5





(C)

Fig. 4.58 Change point analysis of future data for SSP5 (A) Precipitation (B) T max (C) Tmin

The precipitation changes trend early from 2028 onwards in almost all areas across the country and this early changing trend is most visible for the winter season. Some areas of the western India show change during the 2070-2080 timeframe in the summer and monsoon seasons.

The Tmax in almost all regions of India experience change in trend from 2060-2069 whereas during the monsoon season, there is an early change in the trend for the western and eastern ends.

The change in Tmin occurs across the country during the 2062- 2067 in the summers and monsoons whereas for autumn season, there is an earlier change in trend especially towards the eastern side of the midland. During winters also, there is an earlier change in trend (2058-2060) experienced for the whole of western India.

4.4 COMPARISON OF FUTURE TIME SERIES OF METEOROLOGICAL VARIABLE USING WAVELET COHERENCE

The wavelet coherence plot is a valuable technique for investigating the correlation between two signals in both time and meteorological parameters. It provides insights into the dynamic relationships between signals, revealing areas of strong correlation or no

correlation. The wavelet coherence plot brings out a figure with time on the x-axis and frequency of period value on the y-axis. On the right-hand side, the bar indicates the power of the coherence. The yellow colour means higher power, and the blue colour means lower coherence between the terms.

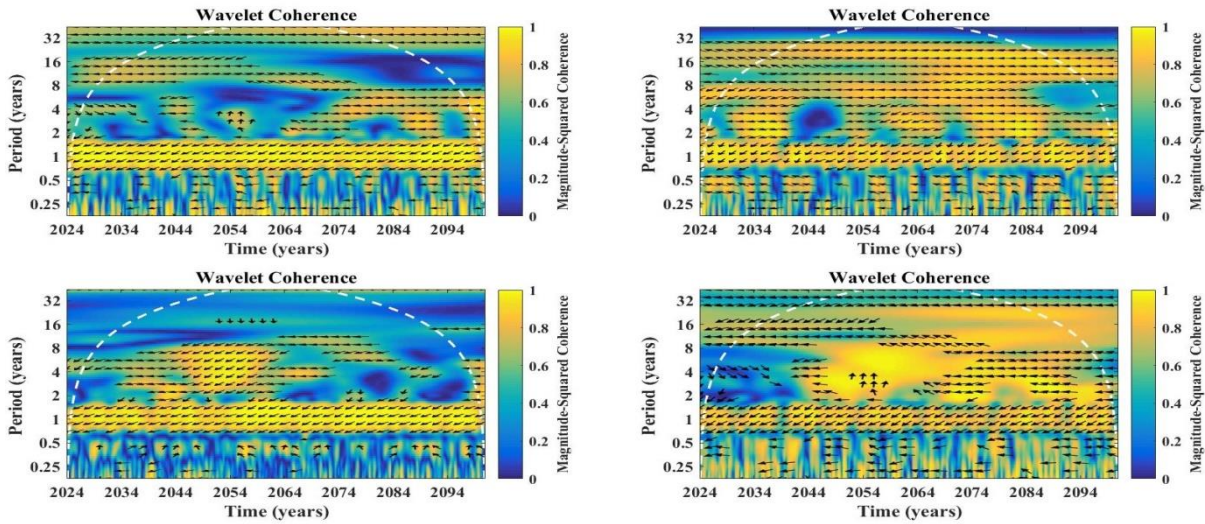


Fig. 4.59 Wavelet coherence plot of region 1- Amw

The precipitation- maximum temperature plot shows that two time series are less correlated in almost all the time intervals and in frequencies, while the maximum correlation is observed upto 2 years in all the scenarios. Moreover, the correlation power is very high for ssp 2-4.5, ssp 3-7.0 and ssp 5-8.5. In almost all significant areas, left pointed arrows suggest negative correlation and up pointed arrows tell that precipitation leads Tmax. The right pointed arrows suggest positive correlation and downward pointed arrows tell that Tmax. leads precipitation.

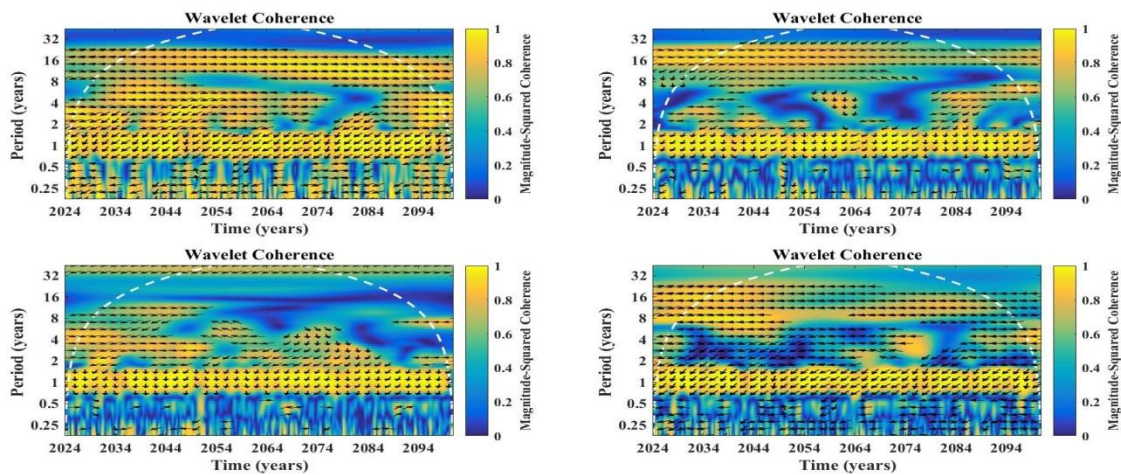


Fig. 4.60 Wavelet coherence plot of region 2- As

The precipitation- maximum temperature plot shows that two time series are more correlated in almost all the time intervals and in frequencies for ssp1-2.6. In case of ssp2-4.5, comparatively, the correlation is observed to have less power whereas in ssp3-7.0, less correlation is observed after 4 years. Ssp 585 shows a similar correlation as of ssp2-4.5 . In almost all significant areas, left pointed arrows suggest negative correlation and up pointed arrows tell that precipitation leads Tmax. The right pointed arrows suggest positive correlation and downward pointed arrows tell that Tmax leads precipitation.

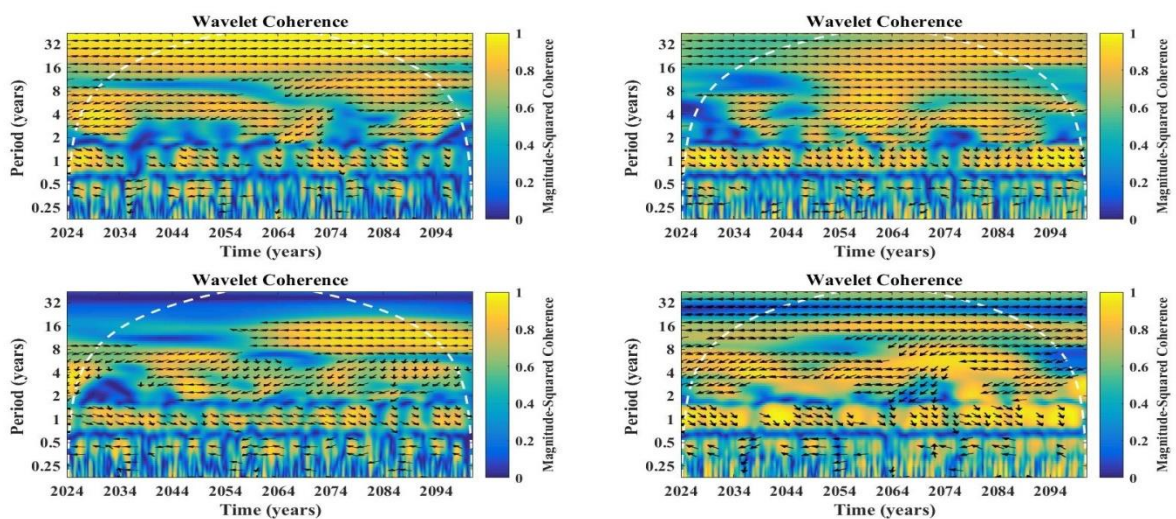


Fig. 4.61 Wavelet coherence plot of region 3- Aw

The precipitation- maximum temperature plot shows that two time series are correlated with high power from 4 to 32 years in the ssp1-2.6 and comparatively less power in the ssp2-4.5. In ssp3-7.0, long term steady correlation is not observed, whereas in the ssp5-8.5, high power correlation is observed. In almost all significant areas, left pointed arrows suggest negative correlation and up pointed arrows tell that precipitation leads Tmax. The right pointed arrows suggest positive correlation and downward pointed arrows tell that Tmax leads precipitation.

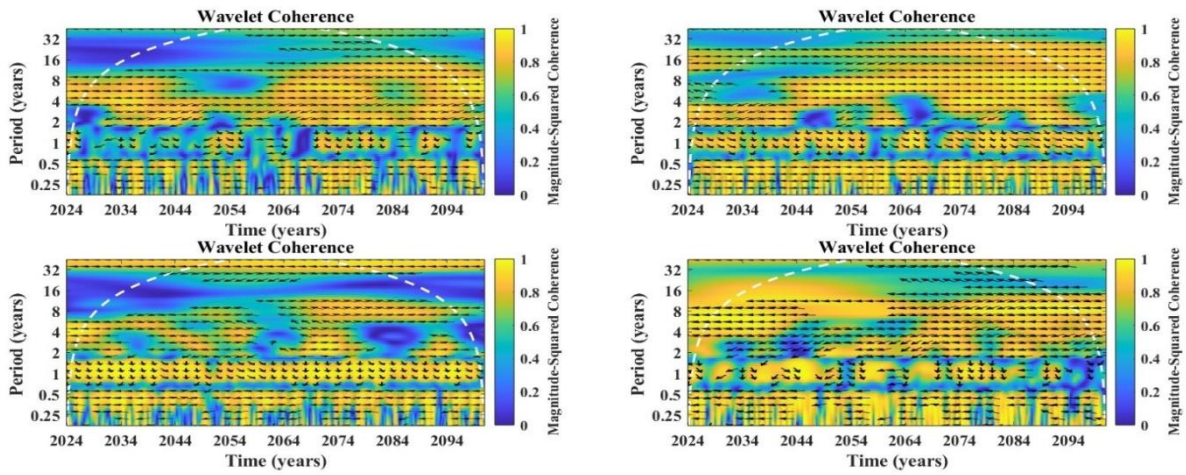


Fig. 4.62 Wavelet coherence plot of region 4- Bshw

The precipitation- maximum temperature plot shows that two time series are correlated with high power in the ssp 245 and ssp 585 and comparatively less power in the ssp1-2.6 and ssp3-7.0 .In ssp1-2.6 and ssp3-7.0, long term steady correlation is not observed. In almost all significant areas, left pointed arrows suggest negative correlation and up pointed arrows tell that precipitation leads Tmax. The right pointed arrows suggest positive correlation and downward pointed arrows tell that Tmax leads precipitation

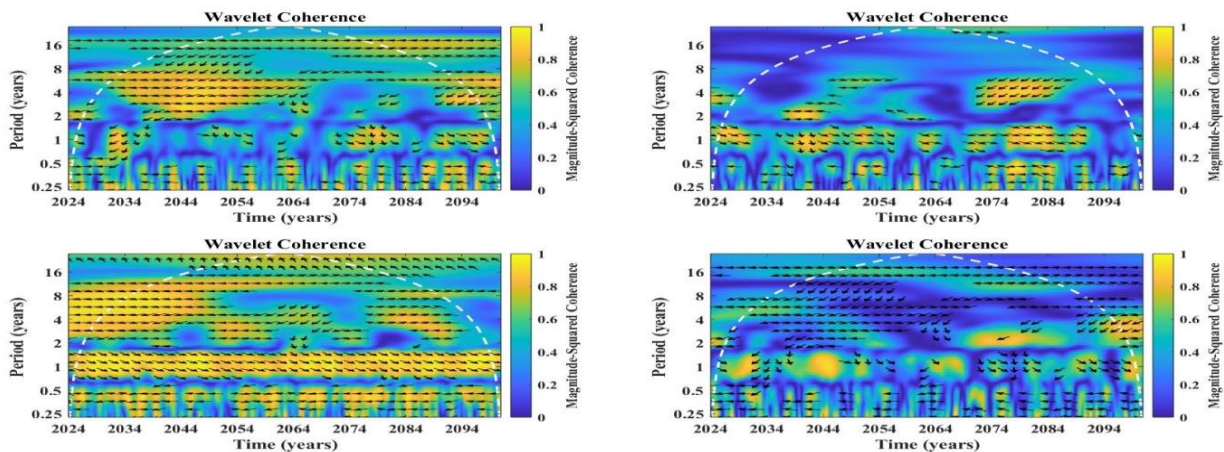


Fig. 4.63 Wavelet coherence plot of region 5- Bwhw

The precipitation- maximum temperature plot shows that two time series are correlated with high power in the ssp1-2.6 and ssp3-7.0 and comparatively less power in the ssp2-4.5 and ssp5-8.5 . In ssp2-4.5 and ssp5-8.5, long term steady correlation is not observed, whereas in the ssp3-7.0, high power correlation is observed. In almost all significant areas, left pointed arrows suggest negative correlation and up pointed arrows tell that precipitation leads Tmax. The right pointed arrows suggest positive correlation and downward pointed arrows tell that Tmax leads precipitation.

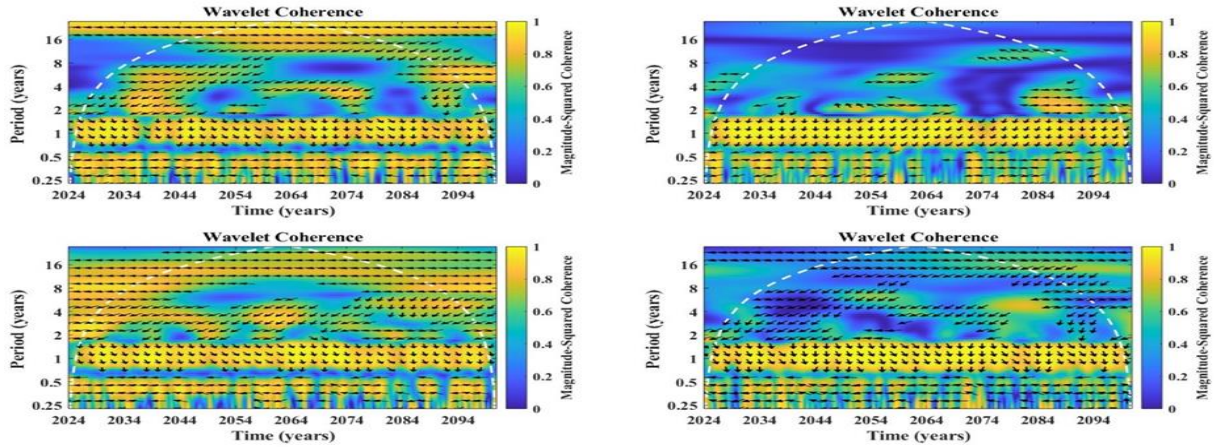


Fig. 4.64 Wavelet coherence plot of region 6- Cwg

The precipitation- maximum temperature plot shows that two time series are highly correlated from 1 to 2 years in all the 4 ssp scenarios. Greater correlation is observed for ssp1-2.6 and ssp3-7.0. In ssp2-4.5 and ssp5-8.5, long term steady correlation is not observed, whereas in the ssp3-7.0, high power correlation is observed. In almost all significant areas, left pointed arrows suggest negative correlation and up pointed arrows tell that precipitation leads Tmax. The right pointed arrows suggest positive correlation and downward pointed arrows tell that Tmax leads precipitation.

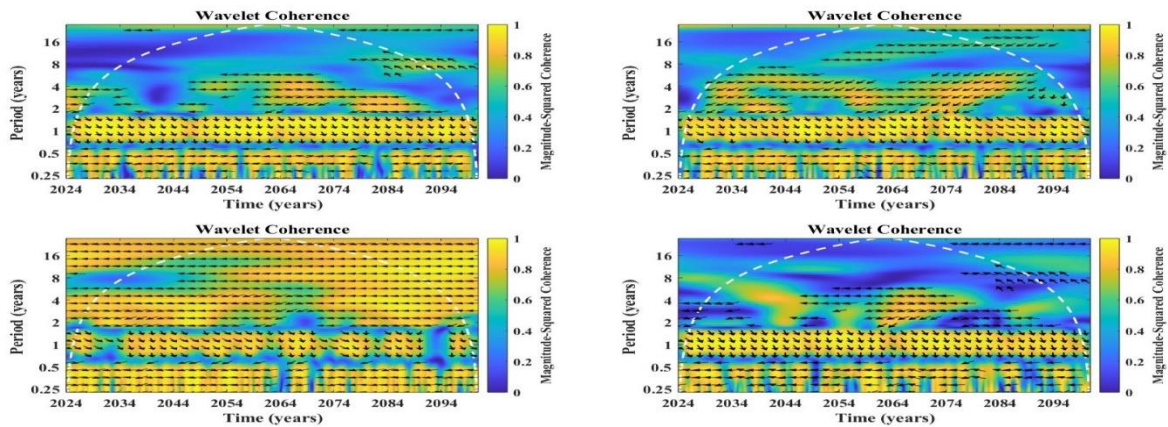


Fig. 4.65 Wavelet coherence plot of region 7- Dfc

The precipitation- maximum temperature plot shows that two time series are correlated in all the 4 ssp scenarios. Greater correlation is observed for ssp3-7.0 throughout the years. In ssp1-2.6, ssp2-4.5 and ssp5-8.5, long term steady correlation is not observed, whereas in the ssp3-7.0, high power correlation is observed. In almost all significant areas, left pointed arrows suggest negative correlation and up pointed arrows

tell that precipitation leads Tmax. The right pointed arrows suggest positive correlation and downward pointed arrows tell that Tmax leads precipitation.

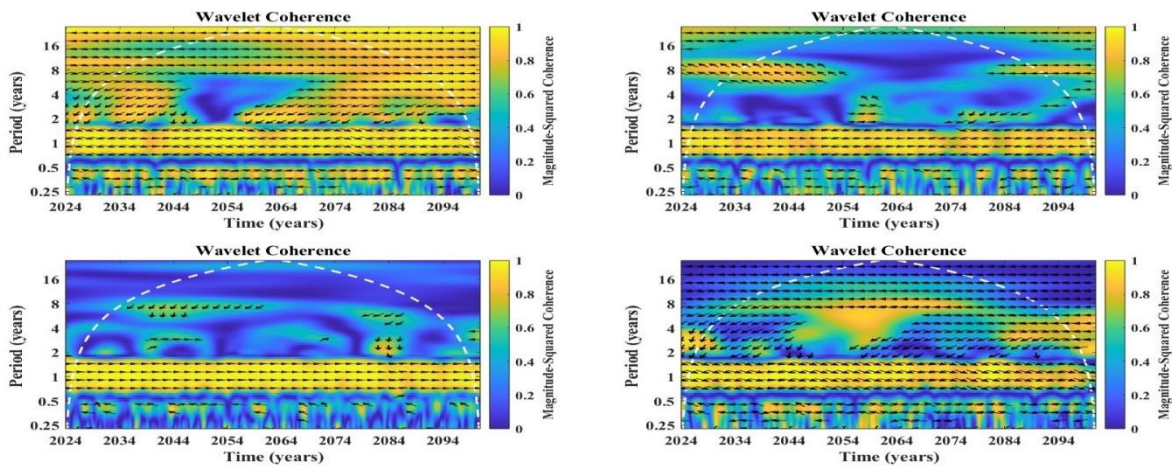


Fig. 4.66 Wavelet coherence plot of region 8- E

The precipitation- maximum temperature plot shows that two time series have high correlation from 1 to 2 years in all the 4 SSP scenarios. Greater correlation is observed for ssp1-2.6. In ssp2-4.5, ssp3-7.0 and ssp5-8.5, long term steady correlation is not observed, whereas in the ssp 126, high power correlation is observed. In almost all significant areas, left pointed arrows suggest negative correlation and up pointed arrows tell that precipitation leads Tmax. The right pointed arrows suggest positive correlation and downward pointed arrows tell that Tmax leads precipitation.

The suitable models for different climatic regions was identified and the trends in the meteorological variables were analysed using the MMK and Sen's slope test. Moreover, the change point detection was done using the Pettit test and the correlation of meteorological variables was analysed through the Wavelet coherence plots.

Summary and conclusion

SUMMARY AND CONCLUSION

In the present study, three key meteorological variables precipitation, maximum and minimum temperature trend pattern were analysed by MMK and SSE statistical tests. For this, future variables were derived from CMIP6 climatic model under four SSP scenarios, while historical data was derived from IMD grid data at fine spatial resolution of $0.25^\circ \times 0.25^\circ$. The suitable models for different climatic regions was identified and the trends in the meteorological variables were analysed using the MMK and Sen's slope test. Moreover, the change point detection was done using the Pettit test and the correlation of meteorological variables was analysed through the Wavelet coherence plots. The main findings of this study are summarized as follows:

1. It was inferred that **ensembled data** is more suitable for the meteorological variable analysis and also found out the suitable models for each climatic region stations other than ensemble data.
2. Precipitation for the last seven decades has shown decreasing trend season to season for year wise except summer. Monsoon precipitation averagely decreased at the rate of -0.0003 mm per season for India.
3. Maximum and minimum temperature increased for all the seasons. Particularly, summer season saw 0.006°C hike each season since mid of the 20th century.
4. For the future time period, precipitation and temperature projected increasing pattern from SSP126 to SSP 586 case. Future monsoon under SSP126 case projected 0.0083 mm rainfall increase for each season, while SSP 586 shows 0.0413 mm per season.
5. Projected summer also appears to be hottest as per SSP 586 case with 0.050°C temperature increase. In the eco-friendly SSP26 scenario, the temperature increase is in the modest level (0.008°C).
6. Like rainfall increase, the variability of rainfall is also more in SSP 586 scenario.
7. Spatially, western region projected more prone to high rainfall variability as well as rainfall decrease.
8. The precipitation- maximum temperature plot shows that two time series are less correlated in almost all the time intervals and in frequencies, while the maximum correlation is observed upto 2 years in all the scenarios

It is further concluded that, high emission scenarios projected high precipitation variation despite increasing pattern, but the eco-friendly SSP126 scenario project the less precipitation variability.

References

REFERENCES

- Abbas, M., Khan, F., Liou, Y.A., Ullah, H., Javed, B. and Ali, S., 2024. Assessment of the impacts of climate change on the construction of homogeneous climatic regions and ensemble climate projections using CMIP6 data over Pakistan. *Atmos. Res.*, *304*, p.107359.
- Ahmed, K., Sachindra, D.A., Shahid, S., Demirel, M.C. and Chung, E.S., 2019. Selection of multi-model ensemble of general circulation models for the simulation of precipitation and maximum and minimum temperature based on spatial assessment metrics. *Hydrol. and Earth Syst. Sci.*, *23(11)*, pp.4803-4824.doi:0.5194/hess-23-4803-2019.
- Alemu, G.T., Desta, S.A. and Tareke, K.A., 2024. Characterize and analysis of meteorological and hydrological drought trends under future climate change conditions in South Wollo, North Wollo, and Oromia Zones, in Ethiopia. *Heliyon*, *10(8)*.
- Animashaun, I.M., Oguntunde, P.G., Akinwumiju, A.S. and Olubanjo, O.O., 2020. Rainfall analysis over the Niger central hydrological area, Nigeria: Variability, trend, and change point detection. *Sci. African*, *8*, p.e00419.
- Araghi, A., Mousavi-Baygi, M., Adamowski, J. and Martinez, C., 2017. Association between three prominent climatic teleconnections and precipitation in Iran using wavelet coherence. *Int.J.of Climatol.*, *37(6)*, pp.2809-2830.
- Bonkaney, A.L., Seidou Sanda, I. and Balogun, A.A., 2019. Wavelet analysis of daily energy demand and weather variables. *J.of Energy*, *2019(1)*, p.4974107.
- Das, J., Jha, S. and Goyal, M.K., 2020. On the relationship of climatic and monsoon teleconnections with monthly precipitation over meteorologically homogenous regions in India: Wavelet & global coherence approaches. *Atmos. Res.*, *238*, p.104889.
- Dawood, M., Rahman, A.U., Ullah, S., Mahmood, S., Rahman, G. and Azam, K., 2020. Spatio-statistical analysis of rainfall fluctuation, anomaly and trend in the Hindu Kush region using ARIMA approach. *Nat. Hazards*, *101*, pp.449-464

- Farboudfam, N., Nourani, V. and Aminnejad, B., 2019. Wavelet-based multi station disaggregation of rainfall time series in mountainous regions. *Hydrol.Res.*, 50(2), pp.545-561.
- Fattah, Md Abdul, Md Mahedi Hasan, Irin Akter Dola, Syed Riad Morshed, Tanmoy Chakraborty, Abdulla-Al Kafy, Saleh Alsulamy, Khaled Mohamed Khedher, and Ahmed Ali A. Shohan. "Implications of rainfall variability on groundwater recharge and sustainable management in South Asian capitals: An in-depth analysis using Mann Kendall tests, continuous wavelet coherence, and innovative trend analysis." *Groundw. for Sustain. Dev.* 24 (2024): 101060.
- Getahun, Y.S., Li, M.H. and Pun, I.F., 2021. Trend and change-point detection analyses of rainfall and temperature over the Awash River basin of Ethiopia. *Heliyon*, 7(9).
- Gocic, M. and Trajkovic, S., 2013. Analysis of precipitation and drought data in Serbia over the period 1980-2010. *J.of Hydrol.*, 494, pp.32-42.
- Goyal, M.K., Gupta, A.K., Jha, S., Rakkasagi, S. and Jain, V., 2022. Climate change impact on precipitation extremes over Indian cities: non-stationary analysis. *Technol. Forecast. and Social Change*, 180, p.121685.
- Guhathakurta, P. and Rajeevan, M., 2008. Trends in the rainfall pattern over India. *International Journal of Climatology: A J.of the R. Meteorol.Society*, 28(11), pp.1453-1469.
- Hu, Q.F. and Wang, Y.T., 2009. Impact assessment of climate change and human activities on annual highest water level of Taihu Lake. *Water Sci.and Eng.*, 2(1), pp.1-15.
- Knutti, R., Furrer, R., Tebaldi, C., Cermak, J. and Meehl, G.A., 2010. Challenges in combining projections from multiple climate models. *J.of Clim.*, 23(10), pp.2739-2758. doi:10.1175/2009JCLI3361.1.
- Koch, J. and Leimbach, M., 2023. SSP economic growth projections: Major changes of key drivers in integrated assessment modelling. *Ecol. Econ.*, 206, p.107751.
- Kumar, S.P., Lahiri, B., Nageswararao, M.M., Alvarado, R. and Sangma, S.N., 2023. Trend analysis and changepoint detection of monthly, seasonal and annual climatic parameters in the Garo Hills of Northeast India. *Ecol.Informatics*, 75, p.102104.

- Li, X., Xu, X., Liu, W., He, L., Xu, C., Zhang, R., Chen, L. and Wang, K., 2019. Revealing the scale-specific influence of meteorological controls on soil water content in a karst depression using wavelet coherency. *Agric.ecosystems & environ.*, 279, pp.89-99
- Mazzoglio, P., Butera, I., Alvioli, M. and Claps, P., 2022. The role of morphology in the spatial distribution of short-duration rainfall extremes in Italy. *Hydrol.and Earth System Sci.*, 26(6), pp.1659-1672.
- Palaniswami, S. and Muthiah, K., 2018. Change point detection and trend analysis of rainfall and temperature series over the Vellar River basin. *Polish J. of Environ.Studies*, 27(4).
- Patel, G., Das, S. and Das, R., 2024. Accuracy of historical precipitation from CMIP6 global climate models under diversified climatic features over India. *Environ. Dev.*, 50, p.100998.
- Petrova, S., 2024. Socio-ecological precarity at the juncture of multiple crises. *Prog.in Hum. Geogr.*, 48(1), pp.35-48.
- Phuong, D.N.D., Duong, T.Q., Liem, N.D., Tram, V.N.Q., Cuong, D.K. and Loi, N.K., 2020. Projections of future climate change in the Vu Gia Thu Bon River Basin, Vietnam by using statistical downscaling model (SDSM). *Water*, 12(3), p.755.
- Pontoppidan, M., Reuder, J., Mayer, S. and Kolstad, E.W., 2017. Downscaling an intense precipitation event in complex terrain: the importance of high grid resolution. *Tellus A: Dyn. Meteorol. and Oceanogr.*, 69(1), p.1271561.
- Rougé, C., Ge, Y. and Cai, X., 2013. Detecting gradual and abrupt changes in hydrological records. *Adv. in Water Resour.*, 53, pp.33-44.
- Sa'adi, Z., Yaseen, Z.M., Farooque, A.A., Mohamad, N.A., Muhammad, M.K.I. and Iqbal, Z., 2023. Long-term trend analysis of extreme climate in Sarawak tropical peatland under the influence of climate change. *Weather and Clim. Extremes*, 40, p.100554.
- Saharwardi, M.S. and Kumar, P., 2022. Future drought changes and associated uncertainty over the homogenous regions of India: a multimodel approach. *Int. J. of Clim.*, 42(1), pp.652-670.doi:10.1002/joc.7265

- Torvanger, A., Henke, C.D. and Marginean, I., 2024. Improving climate risk preparedness-Railroads in Norway. *Clim. Serv.*, 33, p.100439.
- Yadav, J.S., Tiwari, S.K., Misra, A., Rai, S.K. and Yadav, R.K., 2021. High-altitude meteorology of Indian Himalayan Region: complexities, effects, and resolutions. *Environ. Monitoring and Assess.*, 193, pp.1-29.
- Xie, H., Li, D. and Xiong, L., 2014. Exploring the ability of the Pettitt method for detecting change point by Monte Carlo simulation. *Stochastic Environ. Research and Risk Assess.*, 28, pp.1643-1655.
- Xu, F., Zhou, Y. and Zhao, L., 2022. Spatial and temporal variability in extreme precipitation in the Pearl River Basin, China from 1960 to 2018. *Int. J. of Clim.*, 42(2), pp.797-816

APPENDIX- I

Comparison of 13 models as well as the ensembled data among eight stations

Result of the model analysis for the region As

MODELS	As		
	CORRELATION COEFFICIENT	RMSE	MEAN BIAS ERROR
ACCESS-CM2	.51	4.45	-0.01
ACCESS-ESM1-5	.43	5.06	0.01
BCC-CSM2-MR	.18	5.27	0.00
CanESM5	.40	4.95	0.01
EC-Earth3	.50	4.63	0.01
EC-Earth3-Veg	.51	4.519	-0.02
INM-CM4-8	.51	4.54	0.00
INM-CM5-0	.31	5.54	0.00
MPI-ESM1-2-HR	.19	6.28	-0.02
MPI-ESM1-2-LR	.17	6.01	0.00
MRI-ESM2-0	.44	4.92	-0.03
NorESM2-LM	.23	5.48	-0.03
NorESM2-MM	.28	5.32	-0.01
ENSEMBLE	.59	3.74	-0.01

Result of the model analysis for the region Aw

MODELS	Aw		
	CORRELATION COEFFICIENT	RMSE	MEAN BIAS ERROR
ACCESS-CM2	.43	6.03	.09
ACCESS-ESM1-5	.27	6.53	0.13
BCC-CSM2-MR	.61	4.55	0.07
CanESM5	.26	6.55	0.061
EC-Earth3	.64	4.82	0.08

EC-Earth3-Veg	.68	4.63	0.11
INM-CM4-8	.62	5.66	0.09
INM-CM5-0	.63	5.87	0.07
MPI-ESM1-2-HR	.64	4.80	0.06
MPI-ESM1-2-LR	.68	4.57	0.10
MRI-ESM2-0	.62	4.97	0.04
NorESM2-LM	.55	5.45	0.09
NorESM2-MM	.60	5.01	0.09
ENSEMBLE	.79	3.42	0.08

Result of the model analysis for the region Bshw

MODELS	Bshw			
	CORRELATION COEFFICIENT	RMSE	MEAN ERROR	BIAS
ACCESS-CM2	.006	3.116	0.059	
ACCESS-ESM1-5	0.25	3.017	0.036	
BCC-CSM2-MR	0.38	2.69	0.063	
CanESM5	0.03	3.562	0.063	
EC-Earth3	0.31	3.131	0.04	
EC-Earth3-Veg	0.38	3.077	0.043	
INM-CM4-8	0.35	3.247	0.036	
INM-CM5-0	0.29	3.481	0.041	
MPI-ESM1-2-HR	0.26	3.448	0.033	
MPI-ESM1-2-LR	0.26	3.15	0.052	
MRI-ESM2-0	0.24	3.328	0.048	
NorESM2-LM	0.29	3.047	0.06	
NorESM2-MM	0.31	3.025	0.063	

ENSEMBLE	0.52	2.097	0.049
----------	------	-------	-------

Result of the model analysis for the region Bwhw

MODELS	Bwhw			
	CORRELATION COEFFICIENT	RMSE	MEAN ERROR	BIAS
ACCESS-CM2	-0.05	2.24	0.00	
ACCESS-ESM1-5	-0.03	2.39	- 0.005	
BCC-CSM2-MR	0.11	2.02	0.00	
CanESM5	-0.04	2.15	-0.01	
EC-Earth3	0.10	2.27	-0.01	
EC-Earth3-Veg	0.19	2.12	-0.01	
INM-CM4-8	0.12	2.63	0.00	
INM-CM5-0	0.10	2.50	0.00	
MPI-ESM1-2-HR	0.07	2.41	0.01	
MPI-ESM1-2-LR	0.20	2.01	-0.01	
MRI-ESM2-0	-0.01	2.13	-0.02	
NorESM2-LM	0.08	2.25	0.01	
NorESM2-MM	0.08	2.35	0.01	
ENSEMBLE	0.19	1.68	0.00	

Result of the model analysis for the region Cwg

MODELS	Cwg			
	CORRELATION COEFFICIENT	RMSE	MEAN ERROR	BIAS
ACCESS-CM2	0.29	6.29	0.43	
ACCESS-ESM1-5	0.56	5.17	0.40	

BCC-CSM2-MR	0.62	4.32	0.42
CanESM5	-0.20	7.23	0.42
EC-Earth3	0.69	4.25	0.38
EC-Earth3-Veg	0.69	4.46	0.42
INM-CM4-8	0.65	4.47	0.38
INM-CM5-0	0.60	5.11	0.44
MPI-ESM1-2-HR	0.62	4.52	0.40
MPI-ESM1-2-LR	0.62	4.55	0.42
MRI-ESM2-0	0.44	5.12	0.43
NorESM2-LM	0.35	6.54	0.42
NorESM2-MM	0.55	6.54	0.42
ENSEMBLE	0.74	3.47	0.42

Result of the model analysis for the region Dfc

MODELS	Dfc		
	CORRELATION COEFFICIENT	RMSE	MEAN BIAS ERROR
ACCESS-CM2	0.62	7.76	-0.50
ACCESS-ESM1-5	0.58	8.33	-0.44
BCC-CSM2-MR	0.56	8.02	-0.44
CanESM5	0.61	7.84	-0.56
EC-Earth3	0.66	7.87	-0.52
EC-Earth3-Veg	0.69	7.61	-0.55
INM-CM4-8	0.35	11.00	-0.49
INM-CM5-0	0.61	9.93	-0.57
MPI-ESM1-2-HR	0.61	7.83	-0.47
MPI-ESM1-2-LR	0.62	7.77	-0.59

MRI-ESM2-0	0.51	9.26	-0.57
NorESM2-LM	0.66	7.97	-0.46
NorESM2-MM	0.33	11.02	-0.46
ENSEMBLE	0.72	6.52	-0.51

Result of the model analysis for the region E

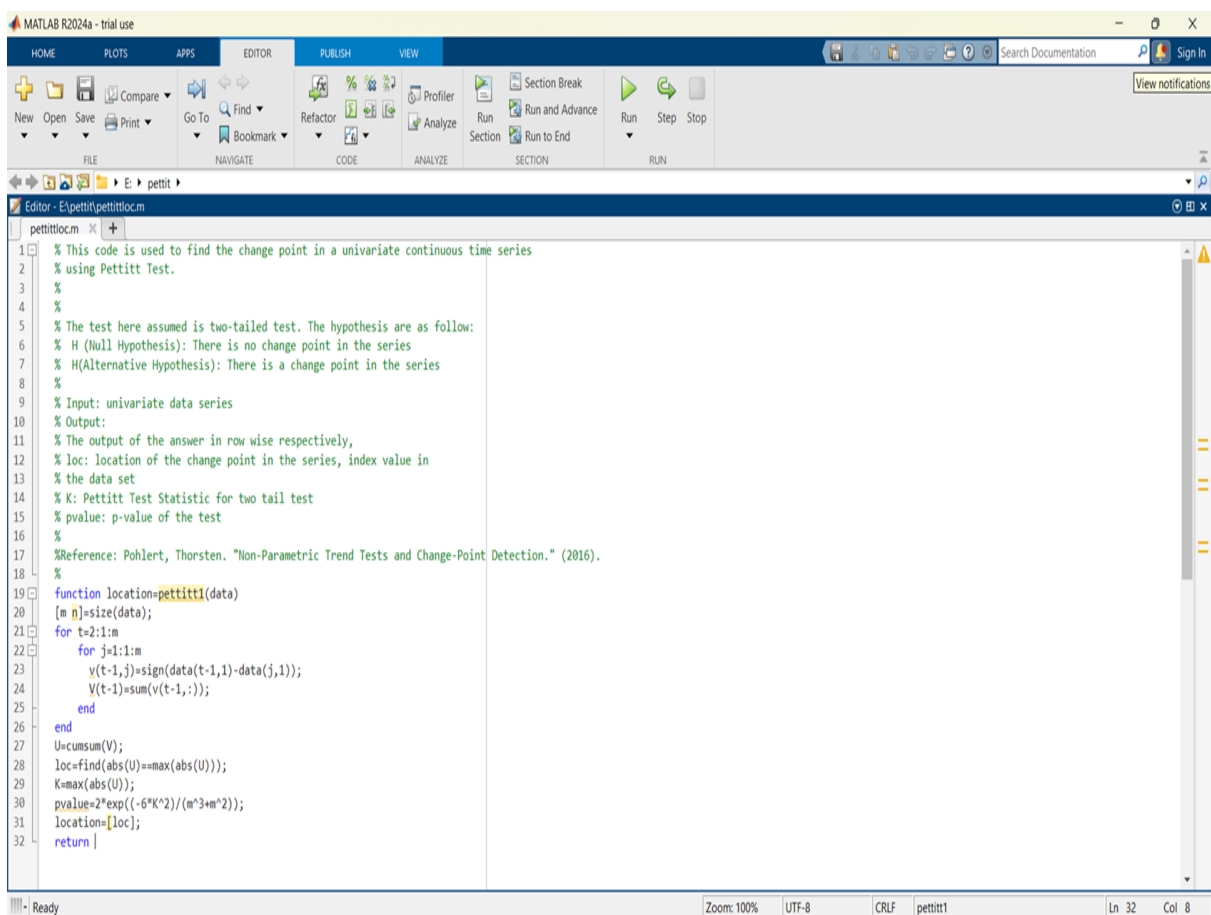
MODELS	E		
	CORRELATION COEFFICIENT	RMSE	MEAN ERROR BIAS
ACCESS-CM2	0.09	3.60	0.63
ACCESS-ESM1-5	0.20	3.88	0.62
BCC-CSM2-MR	0.07	3.20	0.64
CanESM5	-0.16	4.03	0.64
EC-Earth3	0.07	3.26	0.62
EC-Earth3-Veg	0.11	3.27	0.64
INM-CM4-8	0.16	3.52	0.61
INM-CM5-0	0.23	3.38	0.65
MPI-ESM1-2-HR	0.10	3.37	0.64
MPI-ESM1-2-LR	0.23	3.32	0.63
MRI-ESM2-0	0.05	3.46	0.65
NorESM2-LM	0.05	3.73	0.61
NorESM2-MM	0.11	3.67	0.61
ENSEMBLE	0.25	2.62	0.63

APPENDIX- II

MATLAB CODE FOR SEN SLOPE TEST

```
b=[];
for i=1:size(X,2)
    b=[b Sen_Slope(X(:,i))];
end
```

MATLAB CODE FOR PETTITT TEST



The screenshot shows the MATLAB R2024a editor window with the following code for the Pettitt test:

```
1 % This code is used to find the change point in a univariate continuous time series
2 % using Pettitt Test.
3 %
4 %
5 % The test here assumed is two-tailed test. The hypothesis are as follow:
6 % H (Null Hypothesis): There is no change point in the series
7 % H(Alternative Hypothesis): There is a change point in the series
8 %
9 % Input: univariate data series
10 % Output:
11 % The output of the answer in row wise respectively,
12 % loc: location of the change point in the series, index value in
13 % the data set
14 % K: Pettitt Test Statistic for two tail test
15 % pvalue: p-value of the test
16 %
17 %Reference: Pohlert, Thorsten. "Non-Parametric Trend Tests and Change-Point Detection." (2016).
18 %
19 function location=pettitt1(data)
20 [m n]=size(data);
21 for t=2:1:m
22     for j=1:1:m
23         v(t-1,j)=sign(data(t-1,1)-data(j,1));
24         V(t-1)=sum(v(t-1,:));
25     end
26 end
27 U=cumsum(V);
28 loc=find(abs(U)==max(abs(U)));
29 K=max(abs(U));
30 pvalue=2*exp((-6*K^2)/(m^3+m^2));
31 location=[loc];
32 return |
```

The status bar at the bottom indicates: Ready, Zoom: 100%, UTF-8, CRLF, pettitt1, Ln 32, Col 8.

**SPATIO-TEMPORAL ANALYSIS OF METEOROLOGICAL VARIABLES OVER
INDIA FOR 21st CENTURY: APPROACH WITH CMIP6 CLIMATE MODELS**

By

ASHITHA MARIYA SHAJI (2020-02-028)

HARIPRIYA H (2020-02-029)

ANUSHA C RAJESH (2020-02-030)

ADHITHYA P B (2020-02-043)

ABSTRACT

Submitted in partial fulfilment of the requirement for the degree of

Bachelor of Technology

In

Agricultural Engineering

Faculty of Agricultural Engineering and Technology

KERALA AGRICULTURAL UNIVERSITY



**DEPARTMENT OF IRRIGATION AND DRAINAGE ENGINEERING
KELAPPAJI COLLEGE OF AGRICULTURAL ENGINEERING AND
TECHNOLOGY**

TAVANUR-679573, MALAPPURAM

KERALA, INDIA

2024

ABSTRACT

Climate change poses a significant threat to human society, causing loss of livelihoods, human lives, and biodiversity. It affects climatological variables, leading to rising temperatures and precipitation patterns. By the end of the century, global surface temperatures could reach 1.4-5.8°C, increasing disaster severity. According to Germanwatch 2020 report, India is the seventh-most vulnerable nation to climate extremes. Factors such as dense population, diverse climatic regions and huge population engagement at agriculture makes India one of the world's most vulnerable countries.

Through this study suitable climatic models for the eight different regions according to the Koppen's climatic classification was identified by computing Correlation coefficient, Root mean square error and mean bias error. Future changes meteorological variables (precipitation, max and min temperature) simulated from CMIP6 climatic models under four shared socioeconomic pathway scenarios (SSP126, SSP245, SSP370 and SSP585) were evaluated. In this work, the future and historic meteorological variable's trend pattern was investigated with Modified Mann-Kendall (MMK) test and Sen's slope test for the entire India for four different climatic seasons (Monsoon, Autumn, Winter and Summer). The study identified that, for the upcoming future the precipitation and temperature projected increasing trend for all the SSPs. Particularly, SSP 585 case projected relatively more increase than the other scenarios. High precipitation as well as more variability is the case for the SSP 585 scenario. Projected Monsoon and Autumn seasons witnessed more rainfall. Western region of India has more chances of rainfall decrease and risk of dry spell. Over all, remarkable variation of meteorological variable trend between different regions as well as seasons was witnessed over the considered timespan. Moreover the correlation between precipitation and maximum temperature was also analysed using the wavelet coherence plot.